
LONG SHORT-TERM MEMORY EMBEDDED NUDGING SCHEMES FOR NONLINEAR DATA ASSIMILATION OF GEOPHYSICAL FLOWS

Suraj Pawar

School of Mechanical & Aerospace Engineering,
Oklahoma State University,
Stillwater, Oklahoma - 74078, USA.
supawar@okstate.edu

Shady E. Ahmed

School of Mechanical & Aerospace Engineering,
Oklahoma State University,
Stillwater, Oklahoma - 74078, USA.
shady.ahmed@okstate.edu

Omer San

School of Mechanical & Aerospace Engineering,
Oklahoma State University,
Stillwater, Oklahoma - 74078, USA.
osan@okstate.edu

Adil Rasheed

Department of Engineering Cybernetics,
Norwegian University of Science and Technology,
N-7465, Trondheim, Norway.
adil.rasheed@ntnu.no

Ionel M. Navon

Department of Scientific Computing,
Florida State University,
Tallahassee Florida - 32306, USA.
inavon@fsu.edu

ABSTRACT

Reduced rank nonlinear filters are increasingly utilized in data assimilation of geophysical flows, but often require a set of ensemble forward simulations to estimate forecast covariance. On the other hand, predictor-corrector type nudging approaches are still attractive due to their simplicity of implementation when more complex methods need to be avoided. However, optimal estimate of nudging gain matrix might be cumbersome. In this paper, we put forth a fully nonintrusive recurrent neural network approach based on a long short-term memory (LSTM) embedding architecture to estimate the nudging term, which plays a role not only to force the state trajectories to the observations but also acts as a stabilizer. Furthermore, our approach relies on the power of archival data and the trained model can be retrained effectively due to power of transfer learning in any neural network applications. In order to verify the feasibility of the proposed approach, we perform twin experiments using Lorenz 96 system. Our results demonstrate that the proposed LSTM nudging approach yields more accurate estimates than both extended Kalman filter (EKF) and ensemble Kalman filter (EnKF) when only sparse observations are available. With the availability of emerging AI-friendly and modular hardware technologies and heterogeneous computing platforms, we articulate that our simplistic nudging framework turns out to be computationally more efficient than either the EKF or EnKF approaches.

Keywords Nudging method, long short-term memory embedding, transfer learning, extended Kalman filter, ensemble Kalman filter, Lorenz system

1 Introduction

Data assimilation (DA) is a methodology where the observations are utilized to correct the results from a mathematical model to reconstruct spatiotemporal dynamics of a system [1–3]. DA is used extensively for weather forecasting, where there is a growing number of observations coming from satellites, and in situ monitoring. Variational and sequential schemes are two of the most widely used approaches in dynamical data assimilation. For the former, DA is formulated as a minimization problem, where the objective function is defined as the discrepancy between real observations and model's predictions based on a given set of initial conditions and parameters. The argument of this minimization

problem is the set of model’s initial conditions and parameters that need to be tuned to drive the predictions towards the observations. On the other hand, sequential methods usually rely on statistical inference using Bayesian analysis, where the current measurements are used to correct the prior model forecasts to get a better posterior estimate, usually called the analysis in DA terminology.

One of the key limitations of DA methods is that they rely on a forward model whose dynamics is known. For high-dimensional systems like geophysical flows, standard DA methods suffer from the curse of dimensionality. With the increasing resolution of numerical models, the nonlinearities are likely to become so strong that DA algorithms based on linearization might fail [4]. In recent years, with an explosion of data generated from observations, experimental measurements, and numerical simulations, there is a growing interest in applying data-driven methods along with DA [5]. Mostly, efforts focused on using data-driven models in lieu of conventional (physics-based) models in order to accelerate the DA computations. Tang et al. [6] developed a surrogate based model based on convolutional and recurrent neural networks for predicting dynamical subsurface flows and employed it in the DA framework as an emulator to the forward dynamical model. There have been several other studies that demonstrated the potential of data-driven methods in the accurate prediction of complex physical systems such as flooding [7], global atmospheric model [8], quasigeostrophic flows [9], chaotic systems [10, 11], soil water dynamics [12], and tsunami modeling [13]. Recent works have also drawn ideas to synthesize DA with reduced order models [14–23]. Bocquet et al. [24] proposed a hybrid framework by combining DA and machine learning (ML) to estimate the model, the state trajectory, and model error statistics for high-dimensional chaotic systems from partial and noisy observations. Brajard et al. [25] proposed an algorithm where neural networks provide a surrogate forward model to DA and DA provides a time series of complete states to train the neural network. They illustrated the convergence of proposed algorithm for the Lorenz 96 system and achieved the accurate forecasts up to two Lyapunov time units.

Correspondingly, ML tools can also benefit from DA algorithms. Abarbanel et al. [26] offer a perspective on the equivalence between ML and statistical data assimilation and discuss how methods developed in DA can be potentially useful for ML. Bocquet et al. [27] proposed DA as a learning tool to infer ordinary differential equations for dynamical systems solely from noisy data and showed its connection with deep learning methods. Pérez-Ortiz et al. [28] showed that the long short-term memory (LSTM) network can be trained efficiently with better generalization using the decoupled extended Kalman filter [29].

As an extension to the current efforts of using ML tools in DA context, we propose a modular neural-network based DA framework. In other words, we utilize ML to achieve the fusion between the model’s estimates and noisy observations to provide more accurate predictions, rather than using ML as a facilitator to just accelerate existing DA algorithms. To accomplish this, we train a long short-term memory (LSTM) neural network to “nudge” model’s forecast given a set of sparse observations. Nudging is a relatively simple DA approach that uses the forecast error, defined as the difference between model predictions and measurements, to constrain and correct the model evolution. Nudging was introduced by Anthes [30] for the initialization of hurricane models from real observational data. In nudging methods, the state analysis is approximated as a linear superposition between its model forecast and forecast error. Despite its conceptual simplicity, nudging schemes often require adhoc approximation of the nudging (or weighting) matrix. In our framework, we relax this linear superposition assumption and avoid those adhoc approximations by training an LSTM neural network to *nonlinearly* blend model’s forecast and sparse observations.

We demonstrate and test the proposed LSTM-DA framework using the Lorenz 96 system as a benchmark problem in geophysical science applications. We illustrate the success of LSTM-DA using different sets of observations with varying levels of noise and sparsity. In particular, we consider combinations between data-rich, data-deficient, observation-rich, and observation-deficient settings. We also compare our results against some of the common DA techniques. Namely, we discuss the results of extended Kalman filter (EKF), ensemble Kalman filter (EnKF), deterministic ensemble Kalman filter (DEnKF), and a simple forward nudging method. Our LSTM-DA framework can be considered very much similar to the methodology proposed by Zhu et al. [31] in which the fully connected neural network was used to learn the uncertainty in the mathematical model arising from linearization, discretization, and model reduction. The difference in our proposed framework is that we employ the LSTM neural network to learn the nudging correction term in order to cure the discrepancy between prior predictions and measurements that might arise due to inaccurate initial conditions, boundary conditions, or model parameters.

The rest of the manuscript is outlined here. In Section 2, we describe three of the most common nonlinear filtering techniques as benchmarks to compare our framework against. In particular, we briefly outline the extended Kalman filter, which is a first-order adaptation of the standard Kalman filter to deal with nonlinear models. We then introduce the ensemble Kalman filter and its deterministic version as reduced rank variants of nonlinear filters. In Section 3, we discuss the nudging method as a simple alternative to nonlinear filters, which is then extended as a base for our proposed DA-LSTM framework in Section 4. We define the DA set-up using Lorenz 96 system in Section 5. After that, we provide our results in Section 6 as well as relevant discussions and comparisons using different sets of historical data

and observations. Finally, we draw our conclusions as well as the limitations and potential extensions of the present study in Section 7.

2 Nonlinear filtering

The central goal of DA is to extract the information from observational data to correct dynamical models and improve their prediction. There are different approaches such as variational methods like 4D-Var and stochastic methods like ensemble filters that are widely used in DA. Several textbooks on data assimilation offer academic explanations and discussion on these methods [1–3, 32].

In this section, we discuss sequential data assimilation problem and then outline the algorithm procedure for extended Kalman filter (EKF) and ensemble Kalman filter (EnKF). The complete derivation of Kalman filter and its different variants can be found in a number of literature [1–3, 33, 34].

For demonstration, we consider the dynamical system whose evolution is governed by

$$\mathbf{x}_{k+1} = \mathbf{M}(\mathbf{x}_k) + \mathbf{w}_{k+1}, \quad (1)$$

where $\mathbf{x}_k \in \mathbb{R}^n$ is the state of the dynamical system at discrete time t_k , $\mathbf{M} : \mathbb{R}^n \rightarrow \mathbb{R}^n$ is the nonlinear model operator that defines the temporal evolution of the system. The term \mathbf{w}_{k+1} denotes the model noise that takes into account the mathematical model error, numerical approximations, and the boundary conditions. In our study we assume that the model noise is drawn from a multivariate normal distribution with zero mean and a covariance matrix \mathbf{Q}_k , i.e., $\mathbf{w}_k \sim \mathcal{N}(0, \mathbf{Q}_k)$.

Let $\mathbf{z}_k \in \mathbb{R}^m$ be observations of the state vector obtained through noisy measurements procedure as given below

$$\mathbf{z}_k = h(\mathbf{x}_k) + \mathbf{v}_k, \quad (2)$$

where $h(\cdot)$ is a nonlinear function that maps $\mathbb{R}^n \rightarrow \mathbb{R}^m$, also known as the observational operator defining a map between state space and measurement space, and $\mathbf{v}_k \in \mathbb{R}^m$ is the measurement noise. We assume that the measurement noise is a white Gaussian noise with zero mean and the covariance matrix \mathbf{R}_k , i.e., $\mathbf{v}_k \sim \mathcal{N}(0, \mathbf{R}_k)$. Furthermore, we assume that the noise vectors \mathbf{w}_k and \mathbf{v}_k at two different time steps are uncorrelated, which is a common assumption in sequential data assimilation problems. In sequential data assimilation problems, the objective is to estimate the state \mathbf{x}_k given the observations up to time t_k , i.e., $\mathbf{z}_1, \dots, \mathbf{z}_k$. When we use observations to estimate the state of the system, we say that the data are assimilated into the model. There is a number of studies that deal with non-Gaussian distributions for noise vectors [35–37]. However, this is outside the scope of this study and we restrict to assumption of Gaussian noise for model and measurement errors.

We will use the notation $\hat{\mathbf{x}}_k$ to denote an analyzed state of the system at time t_k when all of the observations up to and including time t_k are used in determining the state of the system. When all the observations before (but not including) time t_k are utilized for estimating the state of the system, then we call it the forecast estimate and denote it as \mathbf{x}_k^f . We use the notation \mathbf{P}_k to denote the error covariance matrix. The error covariance matrix for the state vector \mathbf{x}_k is defined as

$$\mathbf{P}_k = \mathbb{E}[(\mathbf{x}_k - \mathbb{E}[\mathbf{x}_k])(\mathbf{x}_k - \mathbb{E}[\mathbf{x}_k])^T], \quad (3)$$

where $\mathbb{E}[\cdot]$ denotes the expected value. We use $\hat{\mathbf{P}}_k$ to denote the error covariance for an analyzed state $\hat{\mathbf{x}}_k$ and \mathbf{P}_k^f denotes the error covariance for the forecast estimate \mathbf{x}_k^f .

Algorithm 1 Extended Kalman filter

1: Initialize the state of the system and error covariance.

$$\hat{\mathbf{x}}_0 = E[\mathbf{x}_0], \quad (4)$$

$$\hat{\mathbf{P}}_0 = \mathbf{P}_0. \quad (5)$$

2: For $k = 0, 1, \dots$ proceed as follow

- Forecast step: Integrate the state estimate and its error covariance from time t_k to t_{k+1} as follow

$$\mathbf{x}_{k+1}^f = \mathbf{M}(\hat{\mathbf{x}}_k), \quad (6)$$

$$\mathbf{P}_{k+1}^f = \mathbf{D}_M \hat{\mathbf{P}}_k \mathbf{D}_M^T + \mathbf{Q}_{k+1}, \quad (7)$$

- Data assimilation step: Once the observations are available at time t_{k+1} , they are incorporated into the state estimate and error covariance estimation as follow

$$\hat{\mathbf{x}}_{k+1} = \mathbf{x}_{k+1}^f + \mathbf{K}[\mathbf{z}_{k+1} - h(\mathbf{x}_{k+1}^f)], \quad (8)$$

$$\mathbf{K} = \mathbf{P}_{k+1}^f \mathbf{D}_h^T [\mathbf{D}_h \mathbf{P}_{k+1}^f \mathbf{D}_h^T + \mathbf{R}_{k+1}]^{-1}, \quad (9)$$

$$\hat{\mathbf{P}}_{k+1} = (\mathbf{I} - \mathbf{K} \mathbf{D}_h) \mathbf{P}_{k+1}^f. \quad (10)$$

2.1 Extended Kalman filter

We first outline the algorithm for extended Kalman filter (EKF) and then discuss in detail its important steps [1]. The procedure for the EKF is summarized in Algorithm 1.

To start with an EKF algorithm, we initialize the state of the system using Equation 4 and error covariance matrix with Equation 5. We evolve the state of the system between two observation points (from time t_k to t_{k+1}) using the known nonlinear dynamics as given in Equation 6. The error covariance matrix is propagated between two observation points using Equation 7. Here $\mathbf{D}_M \in \mathbb{R}^{n \times n}$ is the Jacobian of the model $\mathbf{M}(\cdot)$ and the superscript T denotes the transpose of the matrix. Once the observation \mathbf{z}_{k+1} becomes available at time t_{k+1} , we assimilate it into the forecast state using Equation 8. The matrix $\mathbf{K} \in \mathbb{R}^{n \times m}$ refers to the Kalman gain matrix and is computed as shown in Equation 9, where $\mathbf{D}_h \in \mathbb{R}^{m \times n}$ is the Jacobian of observation function $h(\cdot)$.

The Kalman gain matrix decides the influence of measurements on the estimated state. When the measurement error covariance \mathbf{R}_{k+1} approaches zero, the Kalman gain \mathbf{K} gives more weight to the residual defined as $(\mathbf{z}_{k+1} - h(\mathbf{x}_{k+1}^f))$. On the other hand, when the error covariance \mathbf{P}_{k+1}^f is very small, the Kalman gain \mathbf{K} weights the residual less heavily. Each row of the Kalman gain matrix contains the influence of all observation points on one element of the state \mathbf{x}_{k+1} corresponding to that row. The analyzed error covariance matrix is calculated using Equation 10, where $\mathbf{I} \in \mathbb{R}^{n \times n}$ is an identity matrix.

2.2 Ensemble Kalman filter

When the system is high-dimensional, i.e., n is very large, then the computations for the EKF algorithm are practically infeasible. In addition, the EKF algorithm requires computation of Jacobians and it might be numerically difficult to compute Jacobians for complex models. Ensemble filtering techniques are attractive for such systems where the approximate state of the system is estimated using the standard Monte Carlo framework.

In EKF, the mean estimate of the state $\hat{\mathbf{x}}_k$ and the error covariance matrix $\hat{\mathbf{P}}_k$ are updated sequentially. In contrast to an EKF algorithm, we apply the forecast step to an ensemble of states in the EnKF algorithm [1]. The sample mean and covariance of the ensembles analyses represent the analyzed state estimate $\hat{\mathbf{x}}_k$ and error covariance matrix $\hat{\mathbf{P}}_k$.

Let x_0 be an initial condition drawn from the Gaussian distribution with mean \mathbf{m}_0 and the covariance matrix \mathbf{P}_0 , i.e., $x_0 \sim \mathcal{N}(\mathbf{m}_0, \mathbf{P}_0)$. In our notation we use $\mathbf{X}_k(i)$ to denote the i^{th} member of ensembles and N is the size of ensembles, i.e., $i = 1, 2, \dots, N$. The procedure for the EnKF is summarized in Algorithm 2. We initialize the state of the system for all ensemble members from known distribution of the initial condition for the system as given in Equation 11. Then, we forecast the state of the system for all ensemble members between two observation points (i.e., from time t_k to t_{k+1}) using the nonlinear model dynamics as given in Equation 13. The forecast state estimate and error covariance are

Algorithm 2 Ensemble Kalman filter

1: Initialize the state of the system for different ensemble members.

$$\hat{\mathbf{X}}_0(i) = \mathbf{m}_0 + \mathbf{y}_0(i), \quad (11)$$

$$(12)$$

where $\mathbf{y}_0(i) \sim N(0, \mathbf{P}_0)$.

2: For $k = 0, 1, \dots$ proceed as follow

- Forecast step:

- Integrate the state estimate all ensemble members from time t_k to t_{k+1} as follow

$$\mathbf{X}_{k+1}^f(i) = \mathbf{M}(\hat{\mathbf{X}}_k(i)) + \mathbf{w}_{k+1}. \quad (13)$$

- Compute the sample mean and error covariance as follow

$$\mathbf{x}_{k+1}^f = \frac{1}{N} \sum_{i=1}^N \mathbf{X}_{k+1}^f(i), \quad (14)$$

$$\mathbf{E}_{k+1}^f(i) = \mathbf{X}_{k+1}^f(i) - \mathbf{x}_{k+1}^f, \quad (15)$$

$$\mathbf{P}_{k+1}^f = \frac{1}{N-1} \sum_{i=1}^N \mathbf{E}_{k+1}^f(i) [\mathbf{E}_{k+1}^f(i)]^T. \quad (16)$$

- Data assimilation step:

- Once the observations are available at time t_{k+1} , generate N realizations of virtual observations as follow

$$\mathbf{Z}_{k+1}(i) = \mathbf{z}_{k+1} + \mathbf{v}_{k+1}(i), \quad (17)$$

where $\mathbf{v}_{k+1}(i) \sim N(0, \mathbf{R}_{k+1})$.

- Assimilate the state estimate with virtual observations for all ensemble members as follow

$$\hat{\mathbf{X}}_{k+1}(i) = \mathbf{X}_{k+1}^f(i) + \mathbf{K}[\mathbf{Z}_{k+1}(i) - h(\mathbf{X}_{k+1}^f(i))], \quad (18)$$

$$\mathbf{K} = \mathbf{P}_{k+1}^f \mathbf{D}_h^T [\mathbf{D}_h \mathbf{P}_{k+1}^f \mathbf{D}_h^T + \mathbf{R}_{k+1}]^{-1}. \quad (19)$$

- Compute the sample mean to get analysis state estimate at time t_{k+1}

$$\hat{\mathbf{x}}_{k+1} = \frac{1}{N} \sum_{i=1}^N \hat{\mathbf{X}}_{k+1}(i). \quad (20)$$

calculated based on the sample mean and sample variance of all ensembles as given in Equation 14 and Equation 16, respectively.

Once the observations \mathbf{z}_{k+1} are available at time t_{k+1} , we create N different virtual observations using Equation 17. In the original formulation of EnKF algorithm proposed by Evensen [38], virtual observations were not used in the assimilation step. However, Burgers et al. [39] showed that it is essential to include random perturbations to observations to ensure that the analyzed covariance is not underestimated. Once the virtual observations are generated, the forecast state estimate for all ensembles are assimilated using Equation 18. The Kalman gain \mathbf{K} is computed using the same formula as the EKF algorithm. The analysis state estimate is calculated using the sample mean of analyzed state estimate for all ensemble members as given in Equation 20.

2.3 Deterministic ensemble Kalman filter

Sakov et al. [40] proposed a modification in traditional EnKF that results into matching the analyzed error covariance to that of standard Kalman filter without the need to virtual observations.

Algorithm 3 Deterministic ensemble Kalman filter

1: Initialize the state of the system for different ensemble members.

$$\widehat{\mathbf{X}}_0(i) = \mathbf{m}_0 + \mathbf{y}_0(i), \quad (21)$$

(22)

where $\mathbf{y}_0(i) \sim N(0, \mathbf{P}_0)$.

2: For $k = 0, 1, \dots$ proceed as follow

• Forecast step:

– Integrate the state estimate all ensemble members from time t_k to t_{k+1} as follow

$$\mathbf{X}_{k+1}^f(i) = \mathbf{M}(\widehat{\mathbf{X}}_k(i)) \quad (23)$$

– Compute the sample mean, ensemble anomalies, and error covaraince as follow

$$\mathbf{x}_{k+1}^f = \frac{1}{N} \sum_{i=1}^N \mathbf{X}_{k+1}^f(i), \quad (24)$$

$$\mathbf{A}_{k+1}^f(i) = \mathbf{X}_{k+1}^f(i) - \mathbf{x}_{k+1}^f, \quad (25)$$

$$\mathbf{P}_{k+1}^f = \frac{1}{N-1} \sum_{i=1}^N \mathbf{A}_{k+1}^f(i) [\mathbf{A}_{k+1}^f(i)]^T. \quad (26)$$

• Data assimilation step:

– Once the observations are available at time t_{k+1} , assimilate the forecast state estimate with the observation as follow

$$\widehat{\mathbf{x}}_{k+1} = \mathbf{x}_{k+1}^f + \mathbf{K}[\mathbf{z}_{k+1} - h(\mathbf{x}_{k+1}^f)], \quad (27)$$

$$\mathbf{K} = \mathbf{P}_{k+1}^f \mathbf{D}_h^T [\mathbf{D}_h \mathbf{P}_{k+1}^f \mathbf{D}_h^T + \mathbf{R}_{k+1}]^{-1}. \quad (28)$$

– Compute the analyzed anomalies as below

$$\widehat{\mathbf{A}}_{k+1}(i) = \mathbf{A}_{k+1}^f(i) - \frac{1}{2} \mathbf{K} \mathbf{D}_h \mathbf{A}_{k+1}^f(i). \quad (29)$$

– Calculate the analyzed ensemble using the analyzed state estimate and analyzed anomalies as follow

$$\widehat{\mathbf{X}}_{k+1}(i) = \widehat{\mathbf{A}}_{k+1}(i) + \widehat{\mathbf{x}}_{k+1}. \quad (30)$$

The procedure for the deterministic EnKF (DEnKF) is summarized in Algorithm 3. In practice (e.g., when $n \gg N$), we compute Equation 28 using its square root version (without storing or computing \mathbf{P}_{k+1}^f explicitly) as follows

$$\mathbf{K} = \frac{1}{N-1} \mathbf{A}^f (\mathbf{D}_h \mathbf{A}^f)^T \left[\frac{1}{N-1} (\mathbf{D}_h \mathbf{A}^f) (\mathbf{D}_h \mathbf{A}^f)^T + \mathbf{R}_{k+1} \right]^{-1} \quad (31)$$

where a size of $\mathbb{R}^{n \times N}$ matrix is concatenated as follows

$$\mathbf{A}^f = [\mathbf{A}_{k+1}^f(1), \mathbf{A}_{k+1}^f(2), \dots, \mathbf{A}_{k+1}^f(N)]. \quad (32)$$

In other words, we skip computing Equation 26, and use its reduced-rank square root definition given by

$$\mathbf{P}_{k+1}^f = \frac{1}{N-1} \mathbf{A}^f (\mathbf{A}^f)^T. \quad (33)$$

We start the DEnKF algorithm in a similar manner as the EnKF algorithm by initializing the state estimate for all ensemble members using Equation 21. The anomalies between the forecast estimate of all ensembles and its sample mean is computed utilizing Equation 25. Once the observations are available at time t_{k+1} , the forecast state estimate is

assimilated as given in Equation 27, where the Kalman gain \mathbf{K} is computed in a similar manner as the EKF algorithm. The anomalies for all ensemble members are updated separately with half the Kalman gain. Therefore, the analyzed anomalies for all ensemble members are calculated using Equation 29. The analyzed state estimate for all ensembles members are obtained by offsetting the analyzed anomalies with the analyzed state estimate and is computed using Equation 30.

3 Nudging dynamics

Nudging is another data assimilation method that was introduced by Anthes [30] for initialization of hurricane models from real observational data. Contrary to variational and sequential data assimilation methods that minimize the cost function based on the error between model forecast and observations, nudging methods utilize the forecast error as a constraint to the model evolution equation. The evolution of the dynamical system based on nudging methods can be written as

$$\mathbf{x}_{k+1} = \mathbf{M}(\mathbf{x}_k) + G_k \mathbf{e}_k, \quad (34)$$

where $G_k \in \mathbb{R}^{n \times m}$ is called the time varying nudging coefficient matrix. The forecast error \mathbf{e}_k in Equation 34 is computed as below

$$\mathbf{e}_k = \mathbf{z}_k - h(\mathbf{x}_k). \quad (35)$$

The correction term in Equation 34 is proportional to $\mathbf{e}_k \in \mathbb{R}^m$ (i.e., in the observation space) and therefore this form of nudging is called as observation nudging. The literature on nudging can be divided into different classes/versions based on how the nudging coefficient matrix is computed. Lakshmivaran et al. [41] offer an overview of theoretical aspect of nudging methods and present promising directions of research on the nudging process of dynamic data assimilation. Nudging methods have been applied for different applications such as forecast of Indian Monsoon [42], diagnostic studies of mesoscale processes in mid-latitude weather systems [43, 44], and operational predictions in meteorology and oceanography [45, 46]. Zou et al. [47] proposed a parameter-estimation approach to obtain optimal nudging coefficients using a variational data assimilation method. They estimated the parameters of the nudging coefficient matrix by solving the constrained minimization problem utilizing the Lagrangian formulation. Their cost function consists of two parts, the first part corresponds to the misfit between the model results and observations, and the second part was related to keeping the new estimate of nudging coefficients close to its prior estimate. They enforced the nudged dynamics given in Equation 34 as a strong constraint to the optimization problem. They demonstrated the performance of optimal nudging method for an adiabatic version of the National Meteorological Center (NMC) spectral model with eighteen vertical layers. Vidard et al. [48] introduced another approach to estimate optimal nudging coefficient matrix using the Kalman filter. They illustrated the proposed approach for Burgers equation and shallow-water equations in a twin experiment framework and showed noticeable improvement in the prediction. Auroux et al. [49] introduced the back and forth nudging (BFN) algorithm where the set of observations are incorporated into the model by running it forward in time, starting with some initial condition. After the forward run is completed, the model is again run backward in time, starting from the final state obtained by the standard nudging method. During the backward integration the use of opposite sign for the nudging term as to forward integration makes this algorithm numerically stable. This procedure is repeated in BFN algorithm until the convergence. Therefore, it helps to reduce forecast error on a finite time window. One of the advantage of the BFN algorithm is that it does not require the linearization of nonlinear equations in order to have the adjoint model or to solve any optimization problem. The BFN algorithm was tested for the Lorenz-63 model and for quasi-geostrophic model in the presence of perfect and noisy observations [50] and showed comparable prediction to the 4D-VAR algorithm.

Spectral nudging is another technique where the nudging term is added in the spectral domain with maximum efficiency for large scales and no effect for small scales [51]. This method has been successfully applied to force large-scale atmospheric states from global climate models onto a regional climate model [52–56]. The main idea in spectral nudging is that small-scale details for weather prediction are governed by the interplay between larger-scale atmospheric flow and geographic features like mountains, and land-sea distribution. It is computationally impractical to resolve these small scales in global climate models. Therefore, spectral nudging is applied to match overlapping scales in global and regional climate models by forcing the regional model to behave as global model. Spectral nudging method has also been applied for inferring flow parameters for turbulent flows [57], and for three-dimensional homogeneous isotropic turbulence [58]. There are also nudging methods that make use of present and past observations in the formulation of forcing term to drive the model evolution toward observation [59, 60]. An et al. [61] used the time delayed nudging method [59] for estimating the state of geophysical system from sparse observation data.

4 Long short-term memory nudging

With the huge amount of data generated from high-fidelity numerical simulations, non-invasive experimental techniques like particle image velocimetry (PIV), and satellite data, there is a growing interest in using machine learning for data assimilation [26, 62]. One of the difficulties in weather and climate prediction is that atmospheric flows are multiscale in nature and their dynamics are typically chaotic. Several data-driven algorithms can address these challenges. The recurrent neural networks (RNNs) are particularly attractive for complex dynamical systems due to their ability to capture temporal dependencies and to take state history into account for future state prediction. One of the problems with RNN is that the gradient vanishes during the learning procedure. Long short-term memory [63] is a type of RNN that alleviates this issue of vanishing gradient [64] by employing cell architecture that remembers or forgets information.

There is a rich literature on the application of LSTM for modeling chaotic dynamical systems. Vlachas et al. [11] proposed a data-driven forecasting method for the high-dimensional chaotic system by modeling their temporal dynamics on reduced order space using LSTM. They also integrated the LSTM with a mean stochastic model to ensure convergence and demonstrated its improved prediction performance compared to the Gaussian process. In Wan et al. [65], the LSTM was employed to learn the mismatch between imperfect Galerkin based reduced order model and the actual dynamics projected onto the reduced order space. They showed the improved performance of the proposed framework for the prediction of extreme events. Jia et al. [66] introduced the physics-guided RNN that combines the LSTM and physics-based model to model the dynamics of temperature in lakes. They utilized a physics-based regularization as a penalty term to the optimization cost function to enforce physics into the training. Apart from LSTM, other machine learning algorithms such as reservoir computing have been used for modeling chaotic dynamical systems [10, 67] and residual network for predicting dynamical system evolution [68, 69]. In a recent study, Vlachas et al. [70] investigated the performance of LSTM trained with backpropagation through time and reservoir computing for long term forecasting of chaotic dynamical systems.

Zhang et al. [71] presented an LSTM based Kalman filter for data assimilation of two-dimensional spatio-temporal varying depth of ocean field for underwater glider path planning. In their study, the temporal evolution of spatial basis function was modeled using LSTM. They train the LSTM network to predict the future temporal coefficients based on the historical states of these coefficients. Jin et al. [72] utilized LSTM to perform observation bias correction for data assimilation of dust storm prediction. They showed that with the LSTM model for bias corrections, existing measurements are used precisely and that improves the resulting prediction accuracy. In the work by Loh et al. [73], the LSTM was deployed as a prediction model for their EnKF approach to achieve real-time production forecast in natural gas wells. Xingjian et al. [74] proposed a convolutional LSTM framework to predict the rainfall intensity over a short period of time and illustrated its ability to capture more improved correlation than existing methods.

Motivated by the previous successes of employing neural networks for making better predictions in geophysical applications, in the present study, we introduce an LSTM nudging scheme. The LSTM network is trained to learn the correction term based on the background state of the system and observations. To train the LSTM network, we initialize the state of the system for different training sets from prior distribution of the true initial state. This step is similar to initializing different ensemble members in the case of the EnKF algorithm. We then evolve the system with erroneous initial conditions and compute the correction term using Equation 37 at all observation points. The input features to the LSTM network (denoted by \mathcal{X}_k) consists of full state of the system (from erroneous initial conditions) and current observations, i.e., $\mathcal{X}_k = \{\hat{\mathbf{X}}_k(i); \mathbf{z}_k\} \in \mathbb{R}^{n+m}$, where m is number of observations. Based on these input features, the LSTM is trained to learn the correction term for all states, i.e., the output of the LSTM is $\mathcal{Y}_k = \{\epsilon_k(i)\} \in \mathbb{R}^n$. The LSTM network is capable of capturing the temporal dependencies and utilize it to forecast the system's future state. Therefore, we can also train the LSTM network by including the temporal history of the system's states and observations as input features. Readers are referred to Rahman et al. [9] for further details on incorporating the temporal history of the system's state into training. The procedure for training phase of the LSTM nudging scheme is outlined in Algorithm 4

We adopt the predictor-corrector approach during online deployment. Since the LSTM network is trained to learn the mapping from the state of the system generated with the erroneous initial condition, we start with two systems. We use the superscript E to denote the system with erroneous initial condition and C to denote the evolution of the system whose state is corrected at each observation point. The procedure for online deployment is reported in Algorithm 5. We start with initializing two systems with the same initial condition based on some educated guess. The dynamics of erroneous and corrected systems is evolved simultaneously as given in Equation 43 and Equation 44, respectively. Once the observations are available, we determine the correction term using the trained LSTM network as shown in Equation 45. This correction is for the state of the system generated with the erroneous initial condition. Therefore, the correction is added to the erroneous system's state at that time and assigned to the corrected system. Between two observation points, the corrected system is evolved using this nudged state estimate and we will show that it follows the same trajectory as the true system in Section 6.

Algorithm 4 LSTM Nudging (Training phase)

- 1: Initialize the state of the system for different training sets from prior distribution of $\mathbf{x}_0 \sim N(\mathbf{m}_0, \mathbf{P}_0)$.

$$\hat{\mathbf{X}}_0(i) = \mathbf{m}_0 + \mathbf{y}_0(i), \quad (36)$$

where $\mathbf{y}_0(i) \sim N(0, \mathbf{P}_0)$.

- 2: Integrate the dynamical system and store the system's state at all observation points, i.e., at time t_1, \dots, t_k
3: Compute the correction term at time t_1, \dots, t_k with respect to the true state of the system as follow

$$\boldsymbol{\epsilon}_k(i) = \hat{\mathbf{X}}_k(i) - \bar{\mathbf{x}}_k, \quad (37)$$

where $\bar{\mathbf{x}}_k$ is the true state of the system at t_k .

- 4: Each sample of the input training matrix \mathcal{X}_k and corresponding output data matrix \mathcal{Y}_k is constructed as follow

$$\mathcal{X}_k = \{\hat{\mathbf{X}}_k(i); \mathbf{z}_k\} \in \mathbb{R}^{n+m}, \quad (38)$$

$$\mathcal{Y}_k = \{\boldsymbol{\epsilon}_k(i)\} \in \mathbb{R}^n, \quad (39)$$

where m is the number of observations.

- 5: Train the LSTM model to learn the mapping from input to output

$$\mathcal{M} : \mathcal{X}_k \Rightarrow \mathcal{Y}_k. \quad (40)$$

Algorithm 5 LSTM Nudging (Online deployment)

- 1: Initialize the state of the system for two members with an educated guess for an initial condition.

$$\mathbf{X}_0^E = \mathbf{x}_0, \quad (41)$$

$$\mathbf{X}_0^C = \mathbf{x}_0. \quad (42)$$

- 2: For $k = 0, 1, \dots$ proceed as follow

- Forecast step: Integrate the state estimate for two systems from time t_k to t_{k+1} as follow

$$\mathbf{X}_{k+1}^E = \mathbf{M}(\mathbf{X}_k^E), \quad (43)$$

$$\mathbf{X}_{k+1}^C = \mathbf{M}(\mathbf{X}_k^C). \quad (44)$$

- Data assimilation step: Once the observations are available at time t_{k+1} , they are used to determine the correction term with the trained LSTM network and correct the state estimate as follow

$$\boldsymbol{\epsilon}_{k+1} = \mathcal{M}(\{\mathbf{X}_{k+1}^E; \mathbf{z}_{k+1}\}), \quad (45)$$

$$\mathbf{X}_{k+1}^C = \mathbf{X}_{k+1}^E + \boldsymbol{\epsilon}_{k+1}. \quad (46)$$

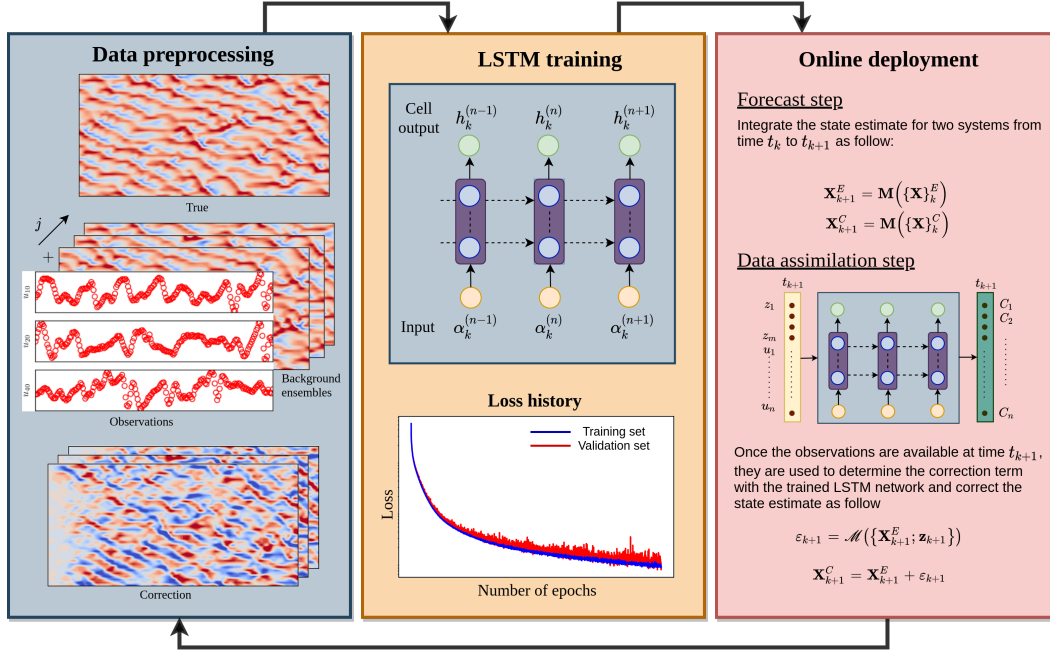


Figure 1: Overview of the LSTM-DA framework. The LSTM-DA framework consists of three main steps: data preprocessing, training the neural network, and the deployment of trained network.

We highlight some of the features of the LSTM nudging framework here. The LSTM nudging framework is highly modular and it can be implemented with other types of neural network architectures also based on the size or type of problems. For example, convolutional autoencoders are gaining popularity to find the nonlinear basis functions of complex physical systems and they are complemented with the LSTM network for learning the latent-space dynamics [75–81]. The LSTM nudging framework can be easily applied to high dimensional systems, where convolutional autoencoders are employed for dimensionality reduction and the LSTM is trained to learn the nudging dynamics in latent-space instead of high-dimensional space. Novel neural network architectures like generative adversarial networks (GANs) [82, 83] can also be applied to learn the nudging dynamics. Another feature of the LSTM nudging scheme is that once the network is trained with the archival or background data, it can be retrained efficiently with transfer learning as the new observation data becomes available. Therefore, training the LSTM network for the first time is the only computationally heavier part of the LSTM nudging scheme. Our main goal in this study is to illustrate that the neural network can be effectively trained to provide accurate and stable nudging dynamics.

5 Data assimilation problem set-up

In this section we describe the Lorenz 96 model proposed by Lorenz [84], which is commonly used as a prototypical test case in data assimilation. This model describes the temporal evolution of atmospheric quantity discretized spatially over a single latitude circle. The system of ordinary differential equation governing the Lorenz 96 model can be written as

$$\frac{du_i}{dt} = u_{i-1}(u_{i+1} - u_{i-2}) - u_i + F, \quad (47)$$

for $i \in \{1, 2, \dots, n\}$. The first term on the right hand side of Equation 47 is the nonlinear advection term, the second term present an internal dissipation, and the third term present an external forcing. We use $n = 40$ and $F = 10$ in our analysis. We apply the periodic boundary conditions at ghost points, i.e., $u_0 = u_n$, $u_{-1} = u_{n-1}$, and $u_{n+1} = u_1$.

We use the fourth-order Runge-Kutta scheme for time integration with a time step of $\Delta t = 0.005$. To generate a physical initial condition for the forward run, we start with an equilibrium condition at time $t = -5$. The equilibrium condition for the model is $u_i = F$ for $i \in \{1, 2, \dots, n\}$. We introduce a very little perturbation to the equilibrium state for the state u_{20} , i.e., we set $u_{20} = F + 0.01$ to generate chaotic dynamics and then do the time integration up to $t = 0$. Once the true initial condition is generated, we run the forward solver up to time $t = 10$.

The twin experiment is one of the most commonly used methods to validate any data assimilation algorithm before it can be applied to real-life applications [85]. For twin experiments, first, we generate the n -dimensional data for the Lorenz 96 model and select m observations. These observations are obtained by adding some noise to the true state of the system to take experimental uncertainties and measurement error into account. The observations are also sparse in time, meaning that the time interval between two observations can be different from the time step of the model. For our twin experiments, we assume that observations are recorded at every 10th time step of the model. Therefore, the time difference between two observations is $\delta t = 0.05$. The analysis time step $\delta t = 0.05$ is representative of six hours of a data assimilation cycle of global meteorological models. The accurate estimation of the full state of the system depends upon the number of observations that are assimilated by the model [86]. We assume that observations locations are constant throughout the time unlike asynchronous observations where they can be rotated [87]. We compare the performance of traditional data assimilation algorithms and the proposed LSTM nudging algorithm for three sets of observations. The first set of observations is very sparse with only 10% of the full state of the system (i.e., $m = 4$), utilizing observations for states $[u_{10}, u_{20}, u_{30}, u_{40}] \in R^4$. In a second set of observations ($m = 8$), we employ observations at $[u_5, u_{10}, \dots, u_{40}] \in R^8$ for the assimilation. The third set of observations consists of 50% of the full state of the system ($m = 20$), i.e., observations at states $[u_2, u_4, \dots, u_{40}] \in R^{20}$ for the assimilation.

6 Results

In this section, we describe the results of numerical experiments with the Lorenz 96 model using algorithms discussed in Section 2, 3 and 4. We assume that our model is perfect for all numerical experiments except for the EKF and EnKF algorithm. For these two algorithms, it is found that an introduction of small uncertainty in the model provides more accurate predictions than the assumption of a perfect model. For the aforementioned two algorithms, we assume that the model noise is drawn from the Gaussian distribution with zero mean and variance 1×10^{-4} . The observations are created by adding random noise from Gaussian distribution with zero mean and variance 1×10^{-2} to the true state of the system. The erroneous initial condition is generated by adding a noise from Gaussian distribution of zero mean and 1×10^{-2} variance to the true initial condition. To ensure a fair comparison between EnKF and DEnKF, we use an equal number of ensembles in both algorithms. For the comparison, we plot time evolution of states u_{10} , u_{21} , u_{39} , and also the full state trajectory of the Lorenz 96 model. We use black lines to denote true states, dashed blue lines to denote states with the erroneous initial condition and dashed-dotted green color lines for assimilated states. The observations for the state u_{10} are shown with red circles in all of the time series plots.

In Figure 2, we present the time evolution of selected states for three different number of observations included in the assimilation of the EKF algorithm. There is an excellent agreement between true and assimilated states u_{21} and u_{39} when more than 20% observations are utilized for assimilation. We also provide the full state trajectory of the Lorenz 96 model in Figure 3. The results obtained clearly show that the EKF algorithm can determine the correct state trajectory with more than 20% observations, i.e., for $m \geq 8$. We observe a discrepancy in prediction after $t \sim 7$, when only four observations are used in the assimilation step. Figure 4 shows the time evolution of selected states predicted by the EnKF algorithm with $N = 40$ ensemble members. We notice some discrepancy between the true and predicted states with $m = 12$ observations after $t \sim 7.5$. If we compare the full state trajectory prediction by the EnKF algorithm in Figure 5, we can conclude that there is almost a perfect match between true and assimilated states with more than 8 observations. Since the EnKF algorithm is based on the Monte Carlo framework, its accuracy can be improved by applying increased number of ensembles. The typical number of ensembles is $O(100)$ for high-dimensional systems [88–90]. Considering that the Lorenz 96 model is a lower-dimensional system with $n = 40$ states, we apply only 40 ensemble members. If we consider the computational cost of the EKF algorithm, the major bottleneck is the propagation of the error covariance matrix as given in Equation 7. The computational overhead of the EnKF algorithm goes up with an increase in the number of ensembles. However, with the advancement in parallel algorithms and high-performance computing, ensemble Kalman filter algorithms are particularly attractive data assimilation of complex physical systems [91].

As we observed in Figure 5, the use of virtual observations in the EnKF algorithm leads to suboptimal performance when fewer observations are used for assimilation with a small number of ensembles. The EnKF data solution converges towards a true solution with an increase in the number of ensembles. The DEnKF algorithm is the deterministic version of the EnKF algorithm where no virtual observations are used. Instead of using virtual observations, the DEnKF algorithm updates the ensemble mean with standard analysis equation and ensemble anomalies are updated separately with half the Kalman gain in the same equation [40]. In Figure 6, we illustrate the time evolution of selected states for different percentages of observations used in the assimilation step. We notice that even with just four observations, the DEnKF algorithm is able to correct the erroneous states up to the final time $t = 10$. From the results depicted in Figure 7, we can deduce that the DEnKF algorithm leads to better performance than the EnKF algorithm when the number of observations is smaller.

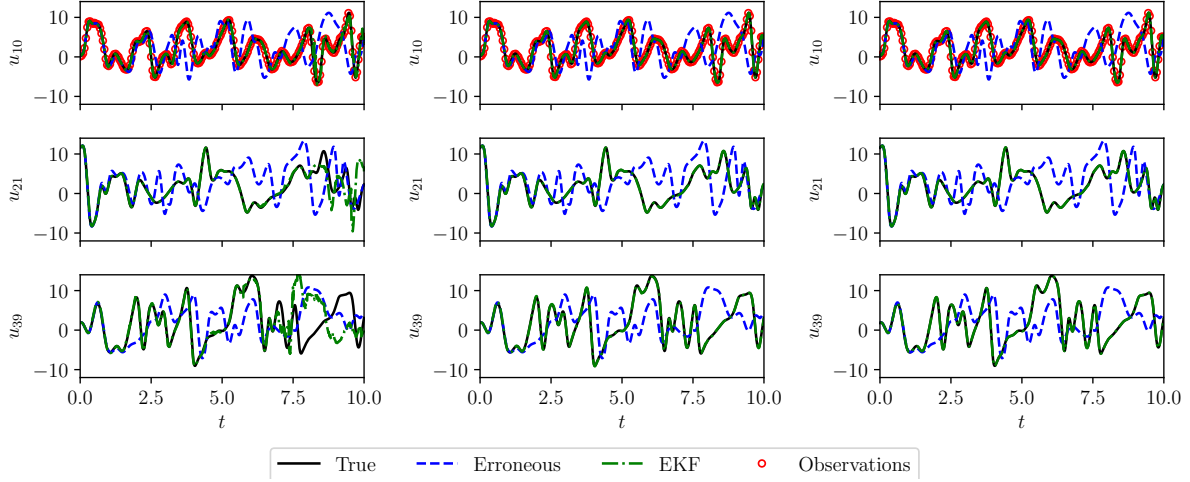


Figure 2: Selected trajectories of the Lorenz 96 model with the analysis performed by the extended Kalman filter (EKF) using observations from $m = 4$ (left), $m = 8$ (middle), and $m = 20$ (right) state variables at every 10 time steps.

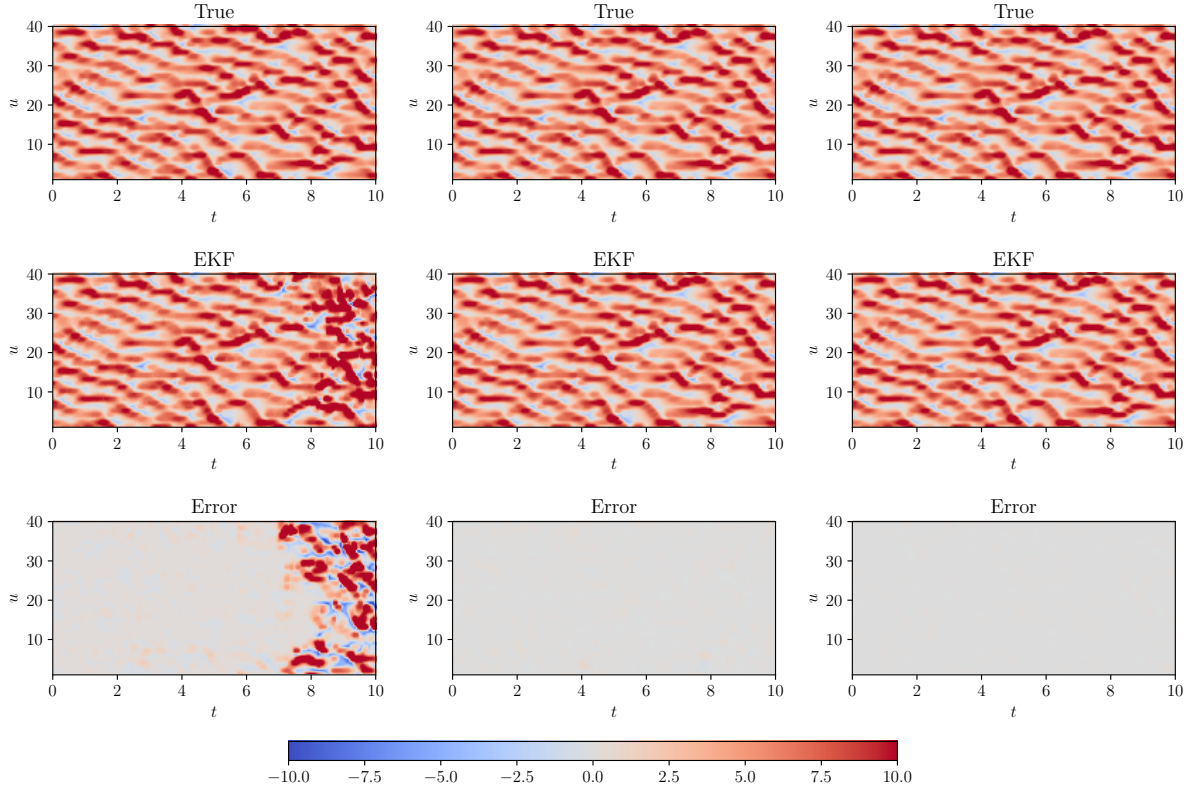


Figure 3: Full state trajectory of the Lorenz 96 model with the analysis performed by the extended Kalman filter (EKF) using observations from $m = 4$ (left), $m = 8$ (middle), and $m = 20$ (right) state variables at every 10 time steps.

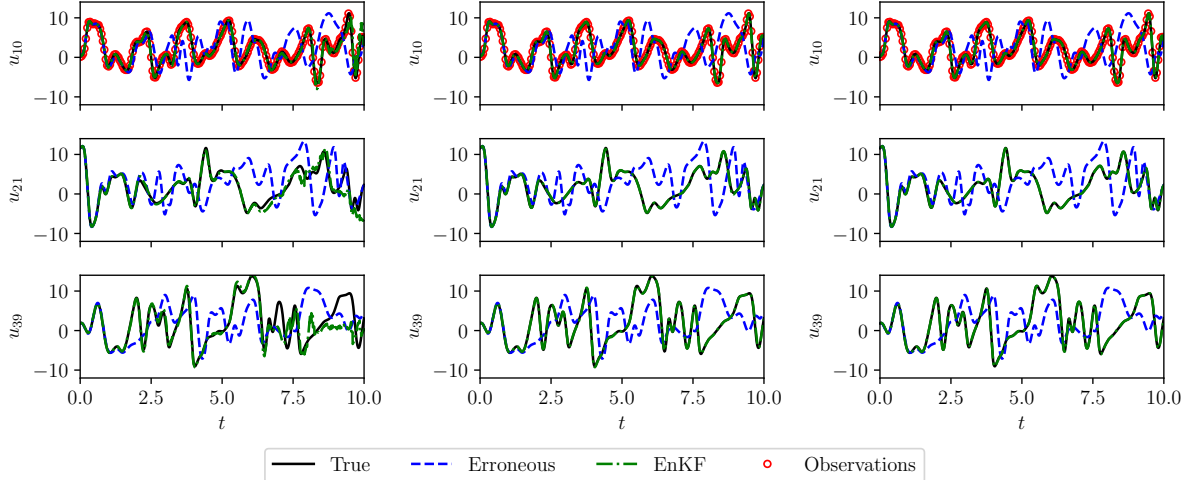


Figure 4: Selected trajectories of the Lorenz 96 model with the analysis performed by the ensemble Kalman filter (EnKF) with $N = 40$ member ensemble using observations from $m = 4$ (left), $m = 8$ (middle), and $m = 20$ (right) state variables at every 10 time steps.

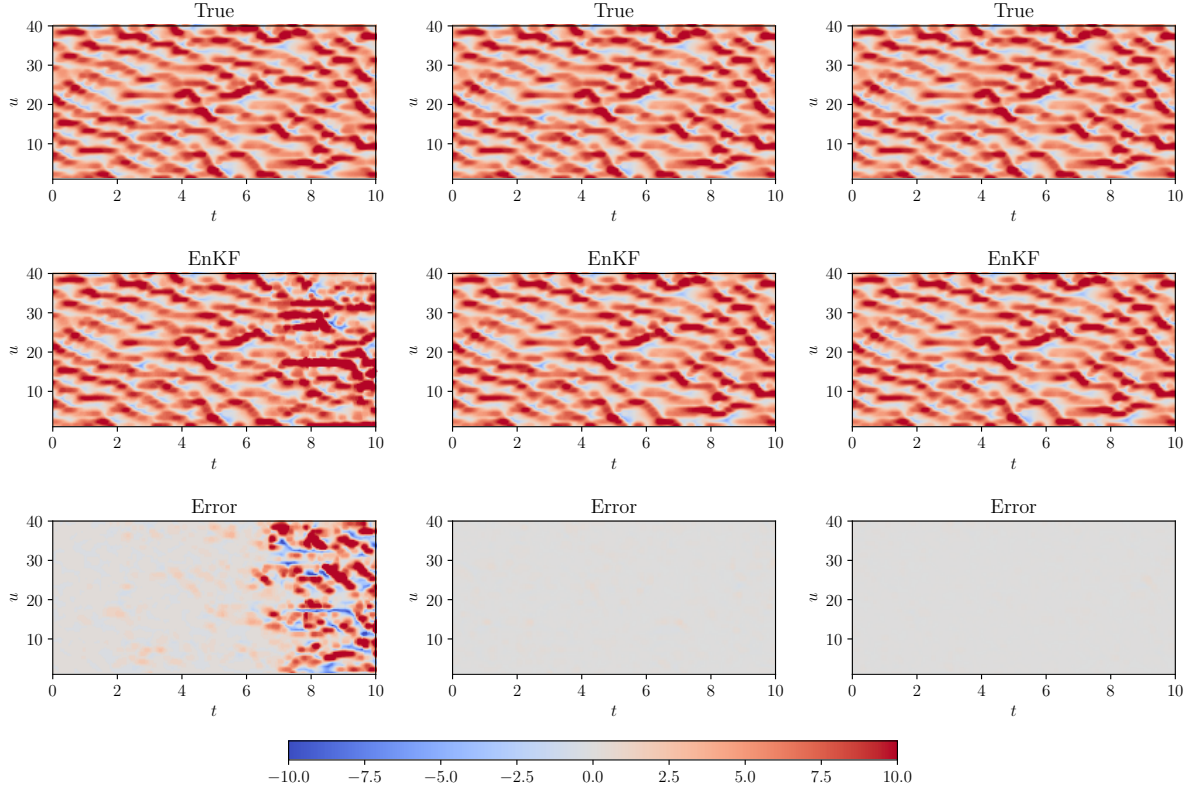


Figure 5: Full state trajectory of the Lorenz 96 model with the analysis performed by the ensemble Kalman filter (EnKF) with $N = 40$ member ensemble using observations from $m = 4$ (left), $m = 8$ (middle), and $m = 20$ (right) state variables at every 10 time steps.

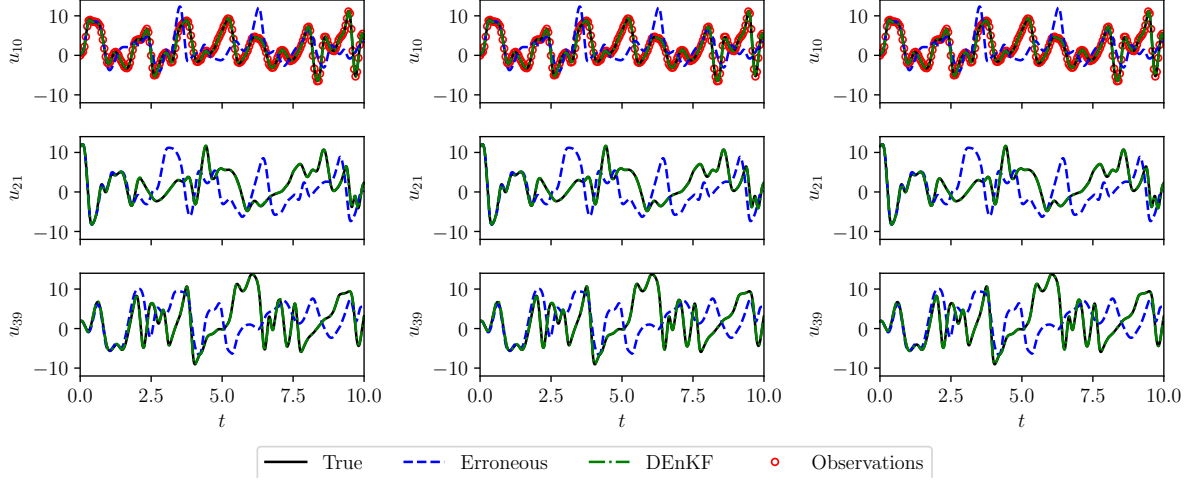


Figure 6: Selected trajectories of the Lorenz 96 model with the analysis performed by the deterministic ensemble Kalman filter (DEnKF) with $N = 40$ member ensemble using observations from $m = 4$ (left), $m = 8$ (middle), and $m = 20$ (right) state variables at every 10 time steps.

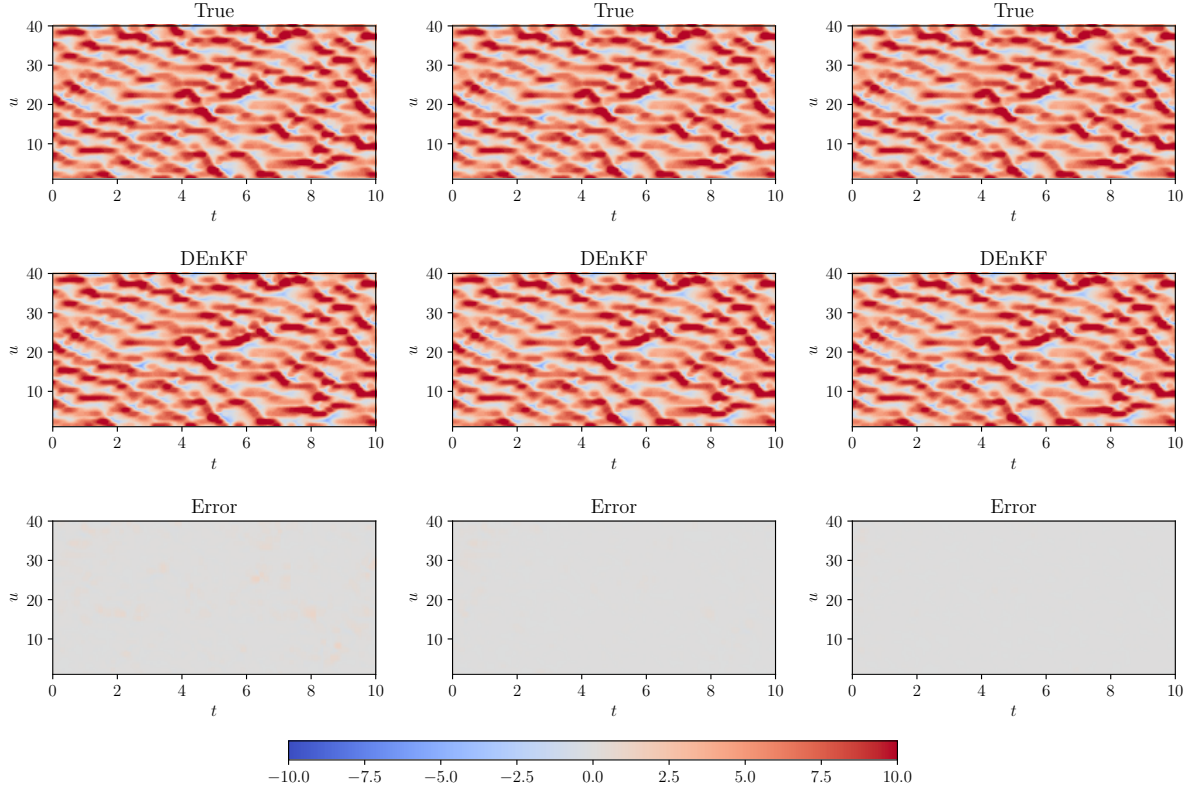


Figure 7: Full state trajectory of the Lorenz 96 model with the analysis performed by the deterministic ensemble Kalman filter (DEnKF) with $N = 40$ member ensemble using observations from $m = 4$ (left), $m = 8$ (middle), and $m = 20$ (right) state variables at every 10 time steps.

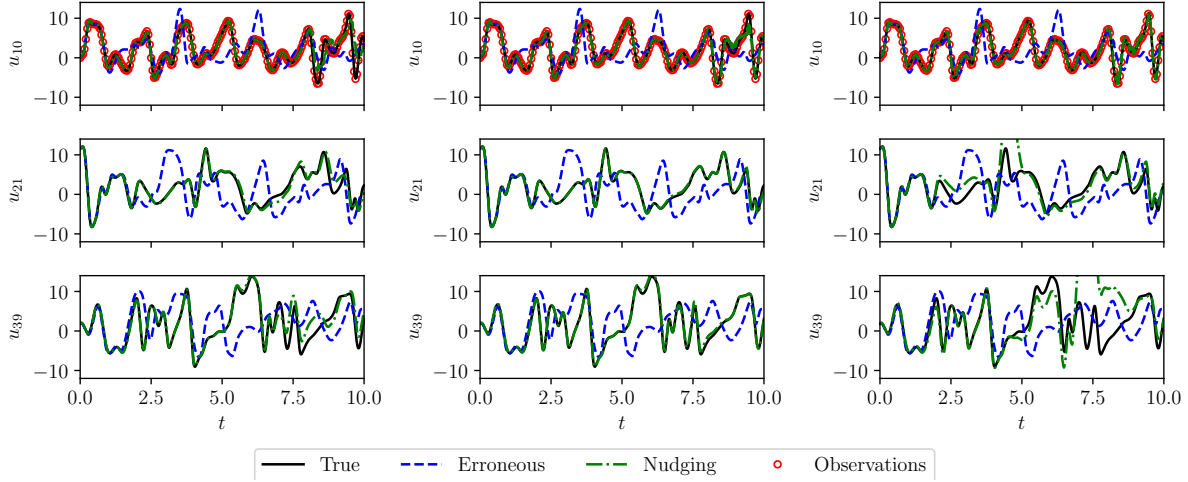


Figure 8: Selected trajectories of the Lorenz 96 model with the analysis performed by the forward nudging with $m = 20$ observations state variables at every 10 time steps for $\tau = 50\Delta t$ (left), $\tau = 100\Delta t$ (middle), and $\tau = 200\Delta t$ (right).

The nonlinear filtering methods discussed in Section 2 are computationally expensive and are prone to curse of dimensionality with an increase in the resolution of the forward numerical model. Nudging methods, on the other hand, are computationally inexpensive and straightforward to implement. As described in Section 3, nudging is accomplished by adding a correction term to the dynamical model which is proportional to the difference between observations and model forecast. One of the main limitations of nudging methods is the adhoc specification of the nudging relaxation coefficient and it is not clear how to choose this coefficient to obtain an optimal solution [92]. Here, we demonstrate how the choice of nudging coefficient affects the prediction when 20 observations are available for assimilation. Since the nudging coefficient represents the relaxation of time scale, we use a constant value for the nudging coefficient that is a function of the time step of the model. Also, the nudging coefficient is assumed to be constant throughout the time integration, i.e., $G_k = \tau$, where τ is a function of the time step of the model. Figure 8 displays the time evolution of selected states for three different values of the nudging coefficient. We notice that for a higher value of τ , the nudging method is not able to correct the model forecast accurately. Figure 9 provides the full state trajectory of the Lorenz 96 model with different nudging coefficient matrix. We observe that the error is sufficiently low at $\tau = 100\Delta t$. Though, the prediction can be further refined by fine-tuning of the nudging coefficient matrix.

Figure 10 and Figure 11 present the time evolution of selected states and full Lorenz 96 system for different number of observations with $\tau = 150\Delta t$. We can easily see that the prediction capability of the nudging scheme is poor when less number of observations are available for the assimilation. Indeed the performance of the nudging scheme can be improved by the optimal specification of nudging coefficient [47], or by using back and forth nudging algorithm [49]. However, the optimal nudging coefficient computation involves obtaining an adjoint model and solving a constrained minimization problem. Also, the back and forth nudging algorithm requires $O(10)$ iterations for convergence and the computational cost will be large for high-dimensional systems. Therefore, machine learning algorithms that are successful in finding the nonlinear mapping between two quantities can be exploited to learn the nudging dynamics.

Now, we describe the results of numerical experiments with the LSTM nudging scheme described in Section 4. For the fair comparison with the EnKF and DEnKF algorithms, we use the data generated from $N = 40$ perturbed initial conditions for the training of the LSTM network. These perturbed initial conditions are created by adding noise from the Gaussian distribution of zero mean and 1×10^{-2} variance to the erroneous initial condition. The training data is obtained by integrating the model with these perturbed initial conditions from time $t = 0$ to $t = 10$ with $dt = 5 \times 10^{-3}$ and then storing the states at all times where observations are present. Therefore, there will be 40,000 samples available for training the LSTM network. The LSTM network is trained using the procedure described in Algorithm 4. We use fairly simple LSTM architecture with two hidden layers consisting of 80 LSTM cells each, and train the network for 2500 epochs. We apply the ReLU activation function and Adam optimizer for the optimization. We found that our training is not highly sensitive to neural network hyperparameters and a similar level of accuracy can be achieved with other sets of hyperparameters. Figure 12 presents the time evolution of selected states for three different number of observations. We see that the LSTM network has learned the mapping from input data to the correction term and is able to produce the correct trajectory even for those states for which observations are not available. In Figure 13, we provide

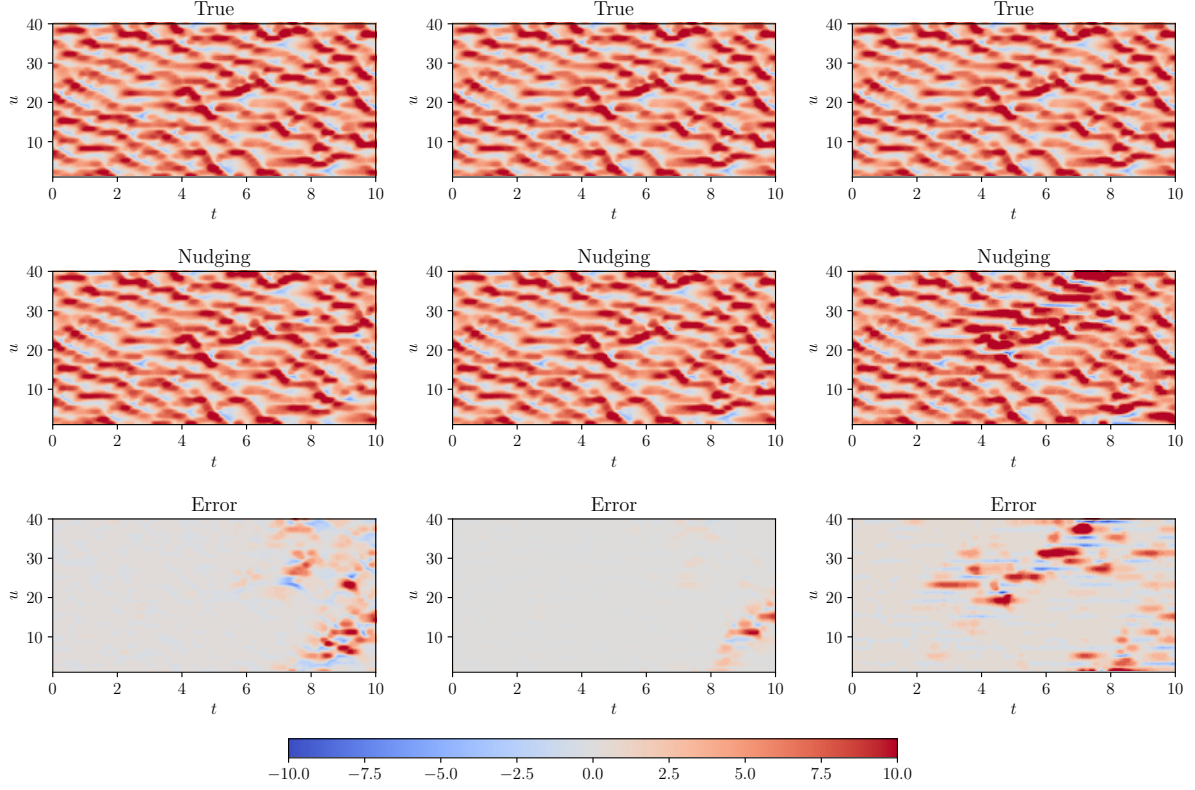


Figure 9: Full state trajectory of the Lorenz 96 model with the analysis performed by the forward nudging with $m = 20$ observations state variables at every 10 time steps for $\tau = 50\Delta t$ (left), $\tau = 100\Delta t$ (middle), and $\tau = 200\Delta t$ (right).

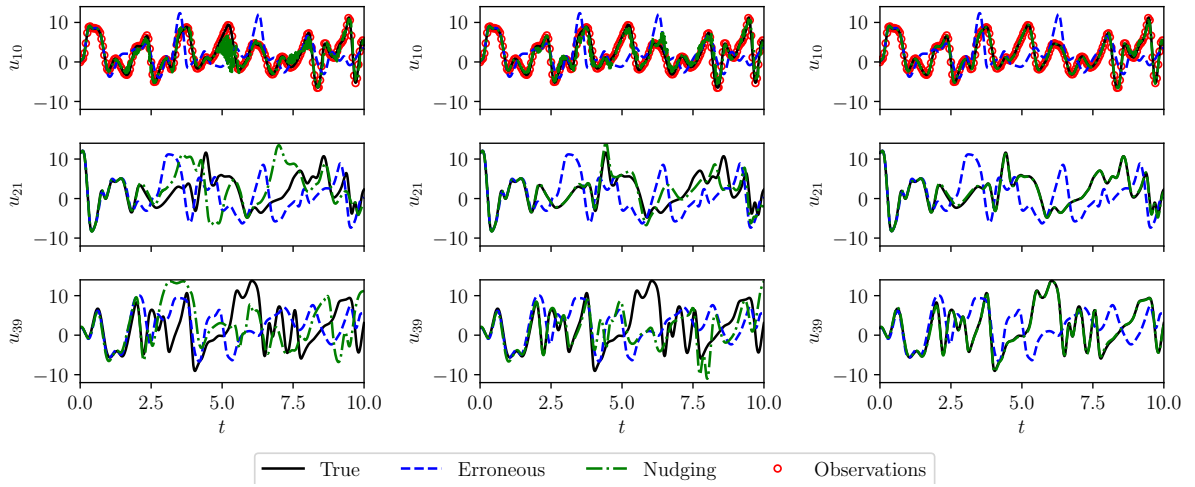


Figure 10: Selected trajectories of the Lorenz 96 model with the analysis performed by the forward nudging with $\tau = 150\Delta t$ using observations from $m = 4$ (left), $m = 8$ (middle), and $m = 20$ (right) state variables at every 10 time steps.

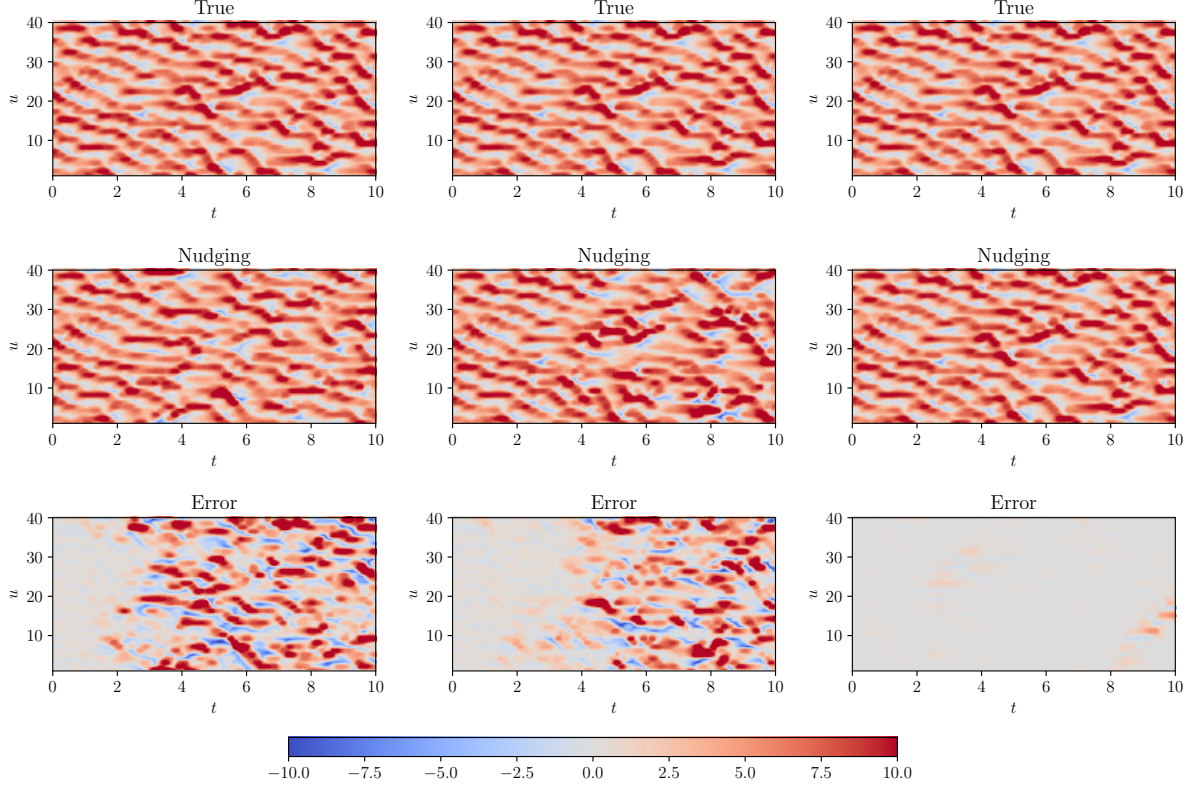


Figure 11: Full state trajectory of the Lorenz 96 model with the analysis performed by the forward nudging with $\tau = 150\Delta t$ using observations from $m = 4$ (left), $m = 8$ (middle), and $m = 20$ (right) state variables at every 10 time steps.

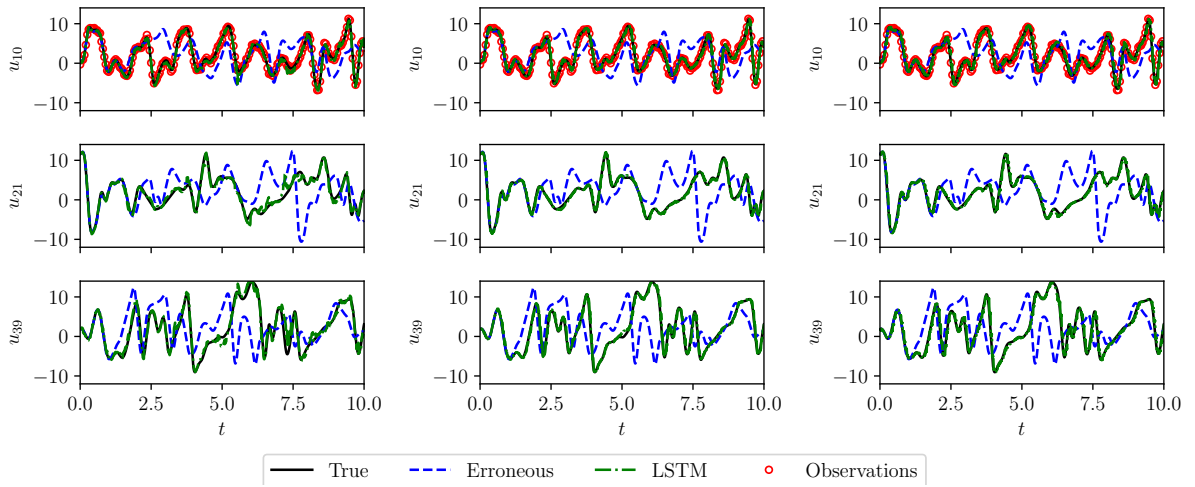


Figure 12: Selected trajectories of the Lorenz 96 model with the analysis performed by the LSTM nudging with $N = 40$ member ensemble for training using observations from $m = 4$ (left), $m = 8$ (middle), and $m = 20$ (right) state variables at every 10 time steps.

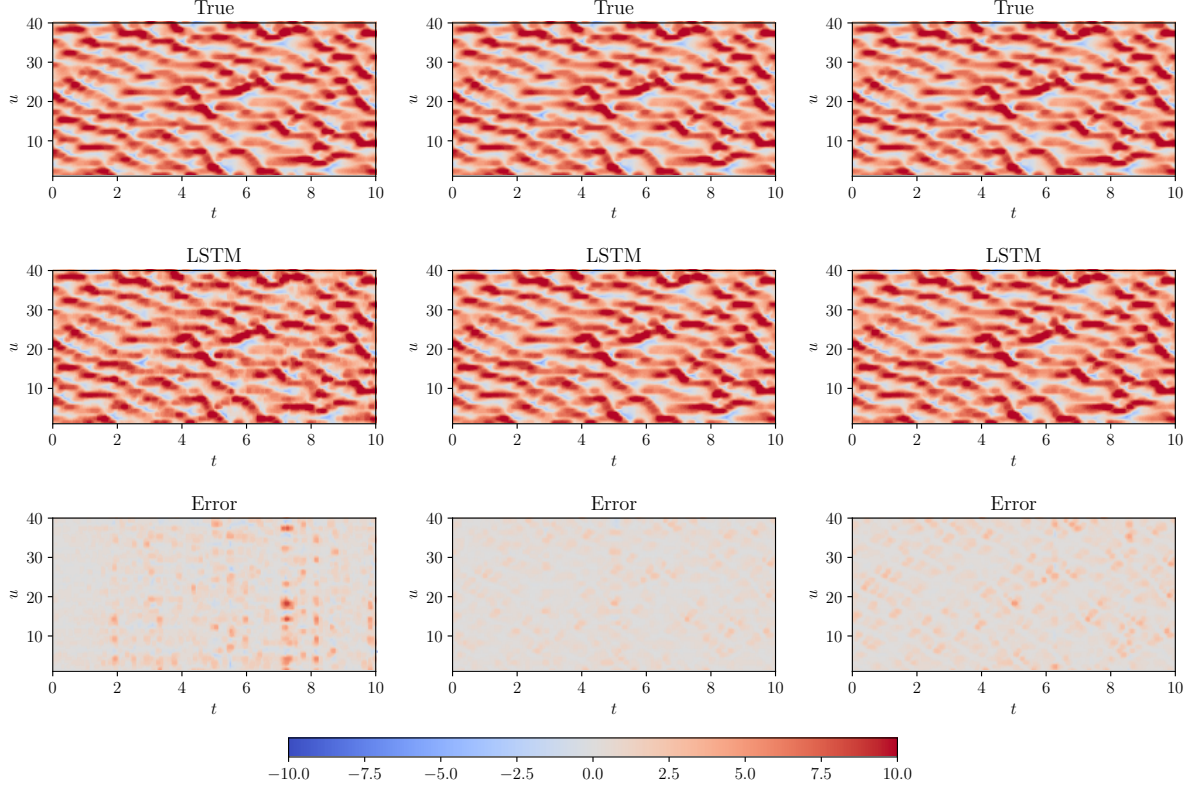


Figure 13: Full state trajectory of the Lorenz 96 model with the analysis performed by the LSTM nudging with $N = 40$ member ensemble for training using observations from $m = 4$ (left), $m = 8$ (middle), and $m = 20$ (right) state variables at every 10 time steps.

the full state trajectory of the Lorenz 96 model for the LSTM nudging method. We get a sufficient level of accuracy comparable to nonlinear filtering algorithms with 20% observations.

From our analysis of numerical experiments with three sets of observations, we can conclude that the LSTM network can learn the nudging dynamics efficiently. Some of the other questions that we want to investigate in this study are; how sparse can the observations be for an accurate prediction?, and how much training data is required for training the network effectively? Figure 14 displays the time evolution selected states for the LSTM nudging scheme with very sparse observations, i.e., $m = 2, 3$, and 4 and we observe a large discrepancy between true and predicted states with less than 10% observations. Figure 15 reports the full state trajectory for the Lorenz 96 model with very sparse observations. The results in Figure 14 and Figure 15 suggests that at least 10% observations are necessary for producing the correct prediction with low error. We point out here that we utilized the data created from only 40 perturbed initial conditions for training, and it is well known that the performance of the neural network can be improved by training with more data.

In Figure 16 and Figure 17, we illustrate the improvement in prediction for highly sparse observations as the amount of data employed for training the LSTM network is increased. We show only the error plot (the difference between true and predicted states) for the conciseness. We can easily observe that the error is large for the EnKF and DEnKF algorithms compared to the LSTM nudging scheme when only two or three observations are available for assimilation. When four observations are present, we see a similar level of accuracy for EnKF, DEnKF, and LSTM nudging method. If we compare the error in Figure 16 and Figure 17, there is an improvement in the prediction as we increase the training data. The results presented in Figure 16 and Figure 17 are obtained by utilizing $N = 200$ and $N = 400$ ensemble members for the EnKF and DEnKF algorithms. The same number of perturbed initial conditions are also used for training the LSTM network. Therefore, in terms of computational cost, all three methods can be considered equivalent because the same number of forward numerical models are integrated from initial time to final time for all three methods. In terms of the storage, the LSTM nudging is more demanding as it requires the storage of full state for all training sets (i.e., perturbed initial condition) at all observation points for the training. However, there is no need to store the solution

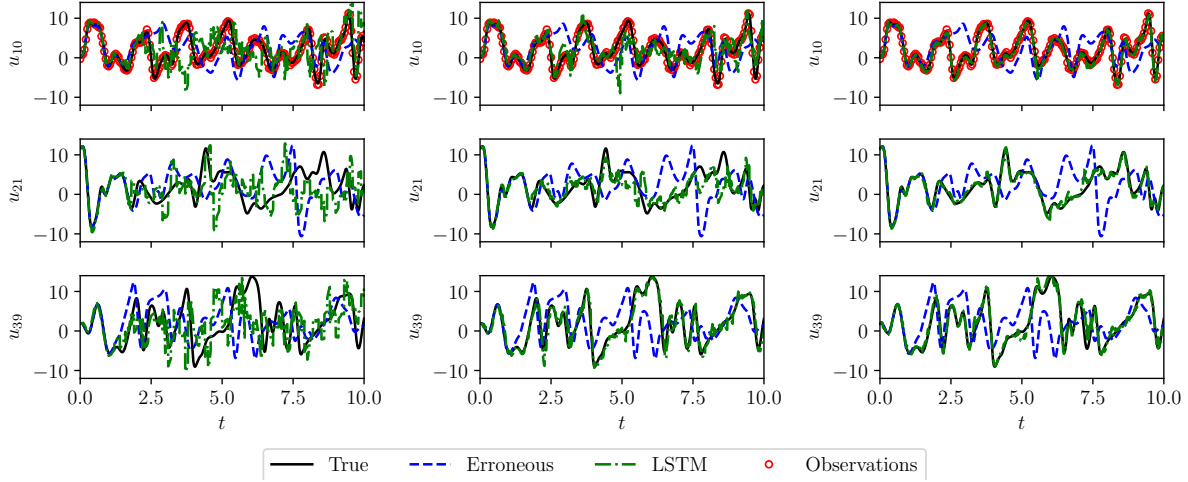


Figure 14: Selected trajectories of the Lorenz 96 model with the analysis performed by the LSTM nudging with $N = 40$ member ensemble for training using observations from $m = 2$ (left), $m = 3$ (middle), and $m = 4$ (right) state variables at every 10 time steps.

of all ensemble members in the EnKF and DEnKF algorithm. This limitation can be addressed by transfer learning, where the weights and biases of the neural network are updated by training its last few layers with new data. Therefore, training the LSTM network for the first time is a computationally intensive task and the LSTM network can be retrained as new observations become available.

7 Conclusions

In the present study, we introduced the LSTM nudging scheme that learns the nudging dynamics from the full state of the system and partial observations. We illustrate the approach for the Lorenz 96 system and compare its performance against extended Kalman filter (EKF), ensemble Kalman filter (EnKF), and deterministic ensemble Kalman filter (DEnKF) approaches. We consider different aspects of the LSTM nudging scheme such as sparsity in observations, and the amount of available data for training the LSTM network. We successfully demonstrate that the LSTM network can be trained to learn the nudging dynamics with extremely sparse observations provided there is a large amount of training data. In terms of computational overhead, training the neural network is the most demanding task. However, this is a one time task and future observations can be incorporated by retraining the neural network with transfer learning at a much less computational cost.

The results of our numerical experiments with the LSTM nudging scheme indicate its potential benefit of assimilation from very sparse observations. Another benefit is that there are no matrix computational operations such as Kalman gain calculation. One of the important caveats of the LSTM nudging scheme is that the neural networks are data-hungry and hence a large amount of archival or background data will be necessary to train the neural network. The suitability of LSTM nudging scheme for DA problems is summarized in Figure 18, where the DA problems are classified based on the sparsity of observations and amount of archival background information. The LSTM nudging scheme is well suited for problems where observations are very sparse and there is the availability of archival background information (i.e., type I problems). Another limitation is that the training procedure in the present form will not be feasible for very high-dimensional systems. One of the solutions to address this constraint is to utilize reduced order modeling (ROM) approaches for dimensionality reduction and recently, machine learning methods are found to give accurate, stable, and robust ROMs for physical systems. Since the LSTM nudging scheme is flexible, we foresee that this approach can be extended to large scale systems by blending it with ROM approaches. One more reservation of the LSTM nudging method is that it does not predict the uncertainty in analyzed states.

We re-emphasize here that the significance of the proposed LSTM nudging method on the prototype model does not mean that they can be directly extended to higher-dimensional and more complex problems. In this work, we assumed that the model is perfect and the noise is Gaussian, which is a very idealized condition. In actual scenarios, real weather forecast models are approximate and contain a lot of parameterizations for subgrid scale processes. Therefore, one can look at the results of numerical experiments presented in this study as the early findings and substantial future

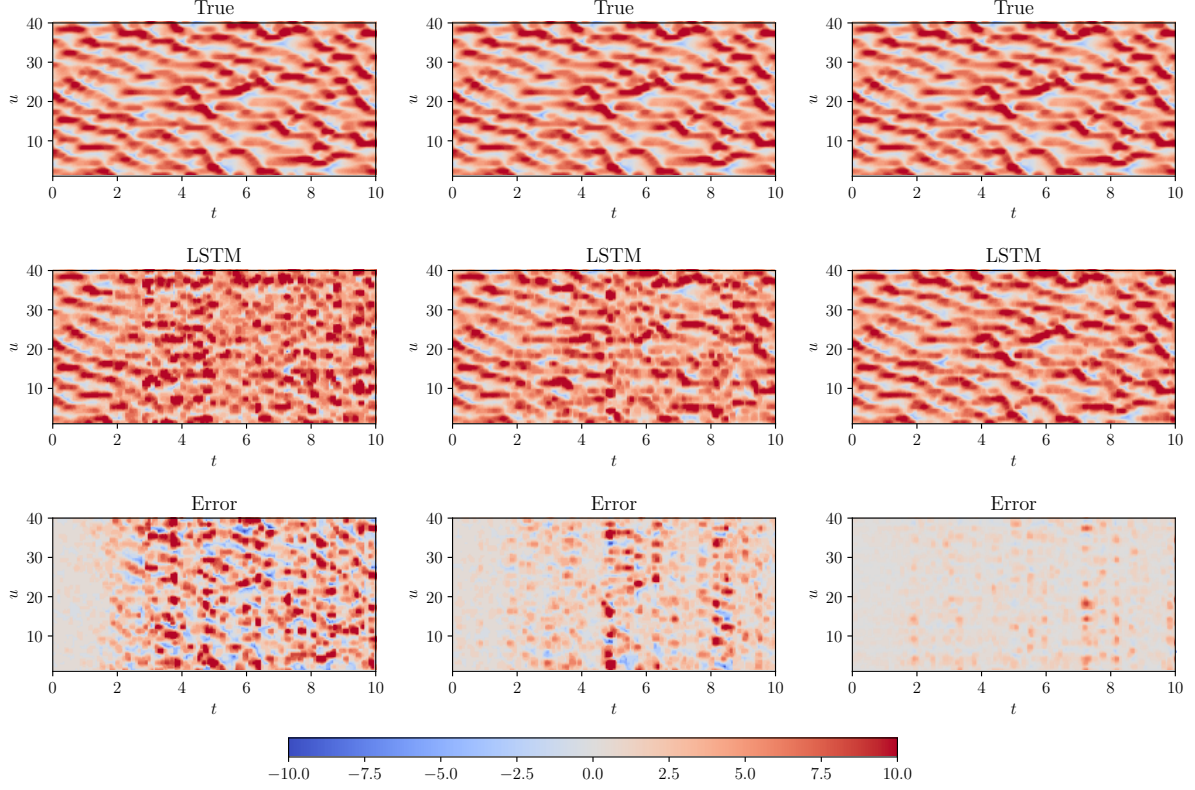


Figure 15: Full state trajectory of the Lorenz 96 model with the analysis performed by the LSTM nudging with $N = 40$ member ensemble for training using observations from $m = 2$ (left), $m = 3$ (middle), and $m = 4$ (right) state variables at every 10 time steps.

work is required for the demonstration of the proposed method in a realistic situation. As a part of future studies, we plan to illustrate the LSTM nudging method for a two-dimensional quasi-geostrophic model with an application of convolutional autoencoder for dimensionality reduction. Neural networks have also been shown to be capable of discovering hidden information about the physical processes embedded in the data [93, 94] and we will integrate these methods with the LSTM nudging scheme for imperfect models.

Acknowledgement

This material is based upon work supported by the U.S. Department of Energy, Office of Science, Office of Advanced Scientific Computing Research under Award Number DE-SC0019290. O.S. gratefully acknowledges their support.

Disclaimer. This report was prepared as an account of work sponsored by an agency of the United States Government. Neither the United States Government nor any agency thereof, nor any of their employees, makes any warranty, express or implied, or assumes any legal liability or responsibility for the accuracy, completeness, or usefulness of any information, apparatus, product, or process disclosed, or represents that its use would not infringe privately owned rights. Reference herein to any specific commercial product, process, or service by trade name, trademark, manufacturer, or otherwise does not necessarily constitute or imply its endorsement, recommendation, or favoring by the United States Government or any agency thereof. The views and opinions of authors expressed herein do not necessarily state or reflect those of the United States Government or any agency thereof.

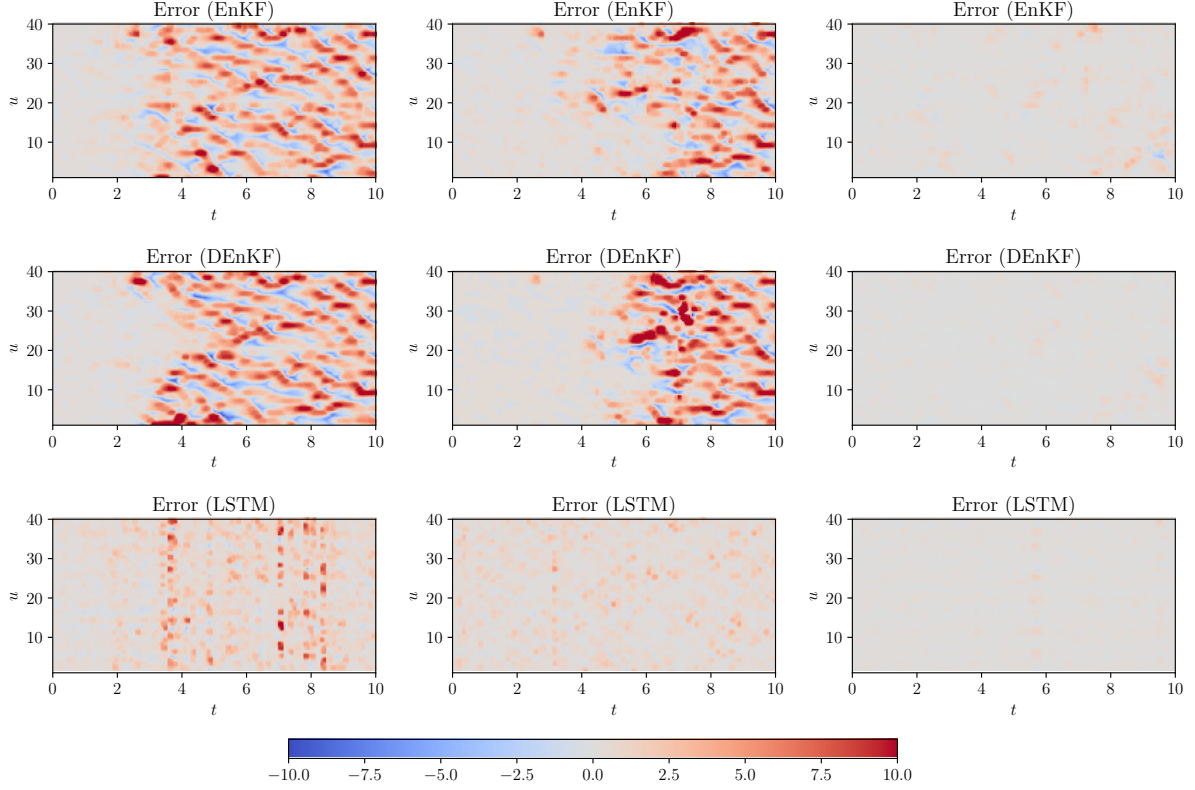


Figure 16: Full state error of the Lorenz 96 model with the analysis performed by the ensemble Kalman filter (EnKF), deterministic ensemble Kalman filter (DEnKF), and LSTM nudging with $N = 200$ member ensemble using observations from $m = 2$ (left), $m = 3$ (middle), and $m = 4$ (right) state variables at every 10 time steps.

A Jacobian of the model and observation matrix

We apply a fourth-order Runge-Kutta (RK4) numerical scheme for temporal integration of the Lorenz 96 model and it can be written as follow

$$\mathbf{u}^{k+1} = \mathbf{u}^k + \frac{\Delta t}{6}(\mathbf{g}_1 + 2\mathbf{g}_2 + 2\mathbf{g}_3 + \mathbf{g}_4), \quad (48)$$

where

$$\mathbf{g}_1 = \mathbf{f}(\mathbf{u}^k), \quad (49)$$

$$\mathbf{g}_2 = \mathbf{f}\left(\mathbf{u}^k + \frac{\Delta t}{2} \cdot \mathbf{g}_1\right), \quad (50)$$

$$\mathbf{g}_3 = \mathbf{f}\left(\mathbf{u}^k + \frac{\Delta t}{2} \cdot \mathbf{g}_2\right), \quad (51)$$

$$\mathbf{g}_4 = \mathbf{f}(\mathbf{u}^k + \Delta t \cdot \mathbf{g}_3). \quad (52)$$

The function \mathbf{f} is the right hand side of the Lorenz 96 model and in the discrete form it can be written as

$$f_i = u_{i-1}(u_{i+1} - u_{i-2}) - u_i + F. \quad (53)$$

The Jacobian of the function \mathbf{f} is defined as below

$$\mathbf{J} = \frac{\partial \mathbf{f}}{\partial \mathbf{u}} = \left[\frac{\partial f_i}{\partial u_j} \right] \quad \text{for } 1 \leq i, j \leq n. \quad (54)$$

The Jacobian \mathbf{J} will be a $\mathbb{R}^{n \times n}$ matrix. The Jacobian of the model $\mathbf{D}_M \in \mathbb{R}^{n \times n}$ can be computed by applying the chain rule to Equation 48 and is given below

$$\mathbf{D}_M = \mathbf{I} + \Delta t \cdot \mathbf{J} + \frac{1}{2}\Delta t^2 \cdot \mathbf{J}^2 + \frac{1}{6}\Delta t^3 \cdot \mathbf{J}^3 + \frac{1}{24}\Delta t^4 \cdot \mathbf{J}^4, \quad (55)$$

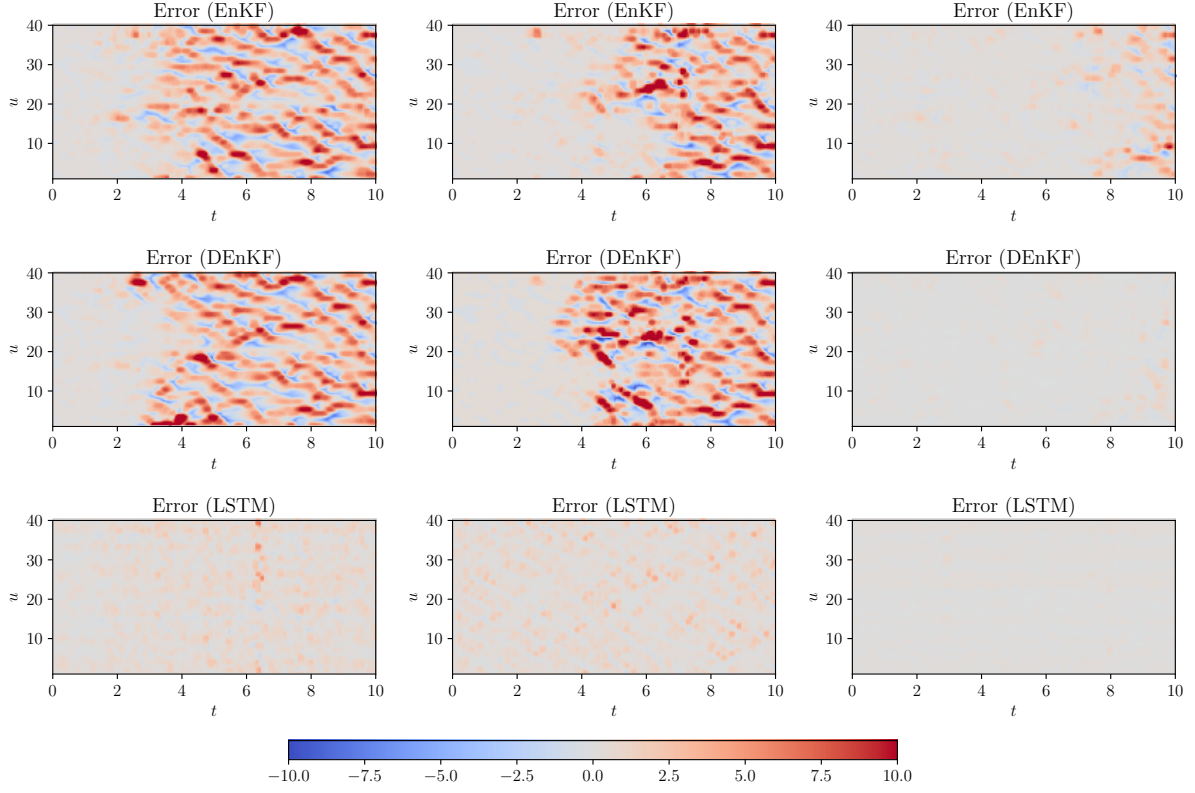


Figure 17: Full state error of the Lorenz 96 model with the analysis performed by the ensemble Kalman filter (EnKF), deterministic ensemble Kalman filter (DEnKF), and LSTM nudging with $N = 400$ member ensemble using observations from $m = 2$ (left), $m = 3$ (middle), and $m = 4$ (right) state variables at every 10 time steps.

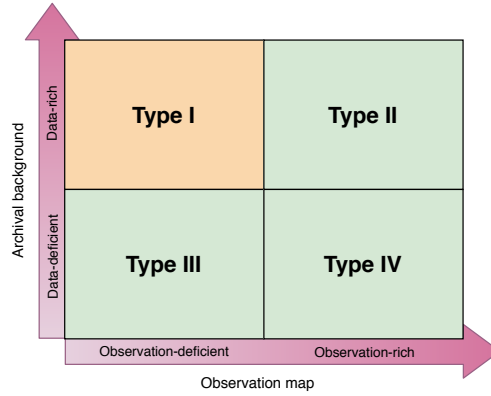


Figure 18: Segregation of problems encountered in data-assimilation based on the observations and archival/ensemble background data. LSTM nudging method is particularly suitable where there is a rich amount archival or background information available for training the network and observations are sparse.

where $\mathbf{I} \in \mathbb{R}^{n \times n}$ is an identity matrix.

The Jacobian of observation is denoted by $\mathbf{D}_h \in \mathbb{R}^{m \times n}$ and is computed as shown below

$$\mathbf{D}_h = \left[\frac{\partial h_i}{\partial u_j} \right], \quad (56)$$

where $1 \leq i \leq m$ and $1 \leq j \leq n$. Since we use linear observations, \mathbf{D}_h will be a constant sparse matrix. Each row of the matrix \mathbf{D}_h will consist of all zeros except for the corresponding observation location, where it will have the value of one.

References

- [1] John M Lewis, Sivaramakrishnan Lakshmivarahan, and Sudarshan Dhall. *Dynamic data assimilation: a least squares approach*, volume 104. Cambridge University Press, 2006.
- [2] Dan Simon. *Optimal state estimation: Kalman, H infinity, and nonlinear approaches*. John Wiley & Sons, 2006.
- [3] Geir Evensen. *Data assimilation: the ensemble Kalman filter*. Springer Science & Business Media, 2009.
- [4] Peter Jan Van Leeuwen. Particle filtering in geophysical systems. *Monthly Weather Review*, 137(12):4089–4114, 2009.
- [5] Redouane Lguensat, Pierre Tandeo, Pierre Ailliot, Manuel Pulido, and Ronan Fablet. The analog data assimilation. *Monthly Weather Review*, 145(10):4093–4107, 2017.
- [6] Meng Tang, Yimin Liu, and Louis J Durlofsky. A deep-learning-based surrogate model for data assimilation in dynamic subsurface flow problems. *arXiv preprint arXiv:1908.05823*, 2019.
- [7] R Hu, F Fang, C C Pain, and I M Navon. Rapid spatio-temporal flood prediction and uncertainty quantification using a deep learning method. *Journal of Hydrology*, 575:911–920, 2019.
- [8] Istvan Szunyogh, Troy Arcomano, Jaideep Pathak, Alexander Wikner, Brian Hunt, and Edward Ott. A machine-learning-based global atmospheric forecast model. 2020.
- [9] Sk Mashfiquir Rahman, Suraj Pawar, Omer San, Adil Rasheed, and Traian Iliescu. Nonintrusive reduced order modeling framework for quasigeostrophic turbulence. *Physical Review E*, 100:053306, 2019.
- [10] Jaideep Pathak, Brian Hunt, Michelle Girvan, Zhixin Lu, and Edward Ott. Model-free prediction of large spatiotemporally chaotic systems from data: A reservoir computing approach. *Physical Review Letters*, 120(2):024102, 2018.
- [11] Pantelis R Vlachas, Wonmin Byeon, Zhong Y Wan, Themistoklis P Sapsis, and Petros Koumoutsakos. Data-driven forecasting of high-dimensional chaotic systems with long short-term memory networks. *Proceedings of the Royal Society A: Mathematical, Physical and Engineering Sciences*, 474(2213):20170844, 2018.
- [12] Peijun Li, Yuanyuan Zha, Liangsheng Shi, Chak-Hau Michael Tso, Yonggen Zhang, and Wenzhi Zeng. Comparison of the use of a physical-based model with data assimilation and machine learning methods for simulating soil water dynamics. *Journal of Hydrology*, 584:124692, 2020.
- [13] M Cheng, F Fang, C C Pain, and I M Navon. Data-driven modelling of nonlinear spatio-temporal fluid flows using a deep convolutional generative adversarial network. *Computer Methods in Applied Mechanics and Engineering*, 365:113000, 2020.
- [14] Bartosz Protas, Bernd R Noack, and Jan Östh. Optimal nonlinear eddy viscosity in Galerkin models of turbulent flows. *Journal of Fluid Mechanics*, 766:337–367, 2015.
- [15] Camille Zerfas, Leo G Rebholz, Michael Schneier, and Traian Iliescu. Continuous data assimilation reduced order models of fluid flow. *Computer Methods in Applied Mechanics and Engineering*, 357:112596, 2019.
- [16] D Xiao, J Du, F Fang, CC Pain, and J Li. Parameterised non-intrusive reduced order methods for ensemble Kalman filter data assimilation. *Computers & Fluids*, 177:69–77, 2018.
- [17] Dacian N Daescu and I Michael Navon. Efficiency of a POD-based reduced second-order adjoint model in 4D-Var data assimilation. *International Journal for Numerical Methods in Fluids*, 53(6):985–1004, 2007.
- [18] Răzvan Ștefănescu, Adrian Sandu, and Ionel Michael Navon. POD/DEIM reduced-order strategies for efficient four dimensional variational data assimilation. *Journal of Computational Physics*, 295:569–595, 2015.
- [19] Yanhua Cao, Jiang Zhu, I Michael Navon, and Zhendong Luo. A reduced-order approach to four-dimensional variational data assimilation using proper orthogonal decomposition. *International Journal for Numerical Methods in Fluids*, 53(10):1571–1583, 2007.

- [20] Céline Robert, S Durbiano, Eric Blayo, Jacques Verron, Jacques Blum, and F-X Le Dimet. A reduced-order strategy for 4d-var data assimilation. *Journal of Marine Systems*, 57(1-2):70–82, 2005.
- [21] Rossella Arcucci, Laetitia Mottet, Christopher Pain, and Yi-Ke Guo. Optimal reduced space for variational data assimilation. *Journal of Computational Physics*, 379:51–69, 2019.
- [22] Steven L Brunton, Bernd R Noack, and Petros Koumoutsakos. Machine learning for fluid mechanics. *Annual Review of Fluid Mechanics*, 52, 2019.
- [23] Vladimir Puzyrev, Mehdi Ghommam, and Shiv Meka. pyROM: A computational framework for reduced order modeling. *Journal of Computational Science*, 30:157–173, 2019.
- [24] Marc Bocquet, Julien Brajard, Alberto Carrassi, and Laurent Bertino. Bayesian inference of chaotic dynamics by merging data assimilation, machine learning and expectation-maximization. *Foundations of Data Science*, 2(1):55, 2020.
- [25] Julien Brajard, Alberto Carrassi, Marc Bocquet, and Laurent Bertino. Combining data assimilation and machine learning to emulate a dynamical model from sparse and noisy observations: a case study with the Lorenz 96 model. *arXiv preprint arXiv:2001.01520*, 2020.
- [26] Henry DI Abarbanel, Paul J Rozdeba, and Sasha Shirman. Machine learning: deepest learning as statistical data assimilation problems. *Neural Computation*, 30(8):2025–2055, 2018.
- [27] Marc Bocquet, Julien Brajard, Alberto Carrassi, and Laurent Bertino. Data assimilation as a learning tool to infer ordinary differential equation representations of dynamical models. *Nonlinear Processes in Geophysics*, 26(3):143–162, 2019.
- [28] Juan Antonio Pérez-Ortiz, Felix A Gers, Douglas Eck, and Jürgen Schmidhuber. Kalman filters improve LSTM network performance in problems unsolvable by traditional recurrent nets. *Neural Networks*, 16(2):241–250, 2003.
- [29] Gintaras V Puskorius and Lee A Feldkamp. Neurocontrol of nonlinear dynamical systems with Kalman filter trained recurrent networks. *IEEE Transactions on Neural Networks*, 5(2):279–297, 1994.
- [30] Richard A Anthes. Data assimilation and initialization of hurricane prediction models. *Journal of the Atmospheric Sciences*, 31(3):702–719, 1974.
- [31] Jiangcheng Zhu, Shuang Hu, Rossella Arcucci, Chao Xu, Jihong Zhu, and Yi-ke Guo. Model error correction in data assimilation by integrating neural networks. *Big Data Mining and Analytics*, 2(2):83–91, 2019.
- [32] Eugenia Kalnay. *Atmospheric modeling, data assimilation and predictability*. Cambridge university press, 2003.
- [33] Arthur Gelb. *Applied optimal estimation*. MIT press, 1974.
- [34] Greg Welch and Gary Bishop. An introduction to the Kalman filter. 1995.
- [35] Weixuan Li, W Steven Rosenthal, and Guang Lin. Trimmed ensemble kalman filter for nonlinear and non-gaussian data assimilation problems. *arXiv preprint arXiv:1808.05465*, 2018.
- [36] Jeffrey L Anderson. A non-Gaussian ensemble filter update for data assimilation. *Monthly Weather Review*, 138(11):4186–4198, 2010.
- [37] Amit Apte, Martin Hairer, A M Stuart, and Jochen Voss. Sampling the posterior: An approach to non-Gaussian data assimilation. *Physica D: Nonlinear Phenomena*, 230(1-2):50–64, 2007.
- [38] Geir Evensen. Sequential data assimilation with a nonlinear quasi-geostrophic model using Monte Carlo methods to forecast error statistics. *Journal of Geophysical Research: Oceans*, 99(C5):10143–10162, 1994.
- [39] Gerrit Burgers, Peter Jan van Leeuwen, and Geir Evensen. Analysis scheme in the ensemble Kalman filter. *Monthly weather review*, 126(6):1719–1724, 1998.
- [40] Pavel Sakov and Peter R Oke. A deterministic formulation of the ensemble Kalman filter: an alternative to ensemble square root filters. *Tellus A: Dynamic Meteorology and Oceanography*, 60(2):361–371, 2008.
- [41] S Lakshmivarahan and John M Lewis. Nudging methods: A critical overview. In *Data Assimilation for Atmospheric, Oceanic and Hydrologic Applications (Vol. II)*, pages 27–57. Springer, 2013.
- [42] TN Krishnamurti, Jishan Xue, HS Bedi, Kevin Ingles, and D Oosterhof. Physical initialization for numerical weather prediction over the tropics. *Tellus B*, 43(4):53–81, 1991.
- [43] David R Stauffer and Nelson L Seaman. Use of four-dimensional data assimilation in a limited-area mesoscale model. part i: Experiments with synoptic-scale data. *Monthly Weather Review*, 118(6):1250–1277, 1990.

- [44] David R Stauffer, Nelson L Seaman, and Francis S Binkowski. Use of four-dimensional data assimilation in a limited-area mesoscale model part ii: effects of data assimilation within the planetary boundary layer. *Monthly Weather Review*, 119(3):734–754, 1991.
- [45] AC Lorenc, RS Bell, and B Macpherson. The meteorological office analysis correction data assimilation scheme. *Quarterly Journal of the Royal Meteorological Society*, 117(497):59–89, 1991.
- [46] John Derber and Anthony Rosati. A global oceanic data assimilation system. *Journal of Physical Oceanography*, 19(9):1333–1347, 1989.
- [47] X Zou, I M Navon, and FX Le Dimet. An optimal nudging data assimilation scheme using parameter estimation. *Quarterly Journal of the Royal Meteorological Society*, 118(508):1163–1186, 1992.
- [48] PA Vidard, FX Le Dimet, and A Piacentini. Determination of optimal nudging coefficients. *Tellus A: Dynamic Meteorology and Oceanography*, 55(1):1–15, 2003.
- [49] Didier Auroux and Jacques Blum. Back and forth nudging algorithm for data assimilation problems. *Comptes Rendus Mathématique*, 340(12):873–878, 2005.
- [50] Didier Auroux and Jacques Blum. A nudging-based data assimilation method: the Back and Forth Nudging (BFN) algorithm. *Nonlinear Processes in Geophysics*, 15:305–319, 2008.
- [51] Kim M Waldron, Jan Paegle, and John D Horel. Sensitivity of a spectrally filtered and nudged limited-area model to outer model options. *Monthly Weather Review*, 124(3):529–547, 1996.
- [52] Hans von Storch, Heike Langenberg, and Frauke Feser. A spectral nudging technique for dynamical downscaling purposes. *Monthly weather review*, 128(10):3664–3673, 2000.
- [53] Raluca Radu, Michel Déqué, and Samuel Somot. Spectral nudging in a spectral regional climate model. *Tellus A: Dynamic Meteorology and Oceanography*, 60(5):898–910, 2008.
- [54] Gonzalo Miguez-Macho, Georgiy L Stenchikov, and Alan Robock. Spectral nudging to eliminate the effects of domain position and geometry in regional climate model simulations. *Journal of Geophysical Research: Atmospheres*, 109(D13), 2004.
- [55] Burkhardt Rockel, Christopher L Castro, Roger A Pielke Sr, Hans von Storch, and Giovanni Leoncini. Dynamical downscaling: Assessment of model system dependent retained and added variability for two different regional climate models. *Journal of Geophysical Research: Atmospheres*, 113(D21), 2008.
- [56] Martina Schubert-Frisius, Frauke Feser, Hans von Storch, and Sebastian Rast. Optimal spectral nudging for global dynamic downscaling. *Monthly Weather Review*, 145(3):909–927, 2017.
- [57] Patricio Clark Di Leoni, Andrea Mazzino, and Luca Biferale. Inferring flow parameters and turbulent configuration with physics-informed data assimilation and spectral nudging. *Physical Review Fluids*, 3(10):104604, 2018.
- [58] Patricio Clark Di Leoni, Andrea Mazzino, and Luca Biferale. Synchronization to big data: Nudging the Navier-Stokes equations for data assimilation of turbulent flows. *Physical Review X*, 10(1):011023, 2020.
- [59] Daniel Rey, Michael Eldridge, Mark Kostuk, Henry DI Abarbanel, Jan Schumann-Bischoff, and Ulrich Parlitz. Accurate state and parameter estimation in nonlinear systems with sparse observations. *Physics Letters A*, 378(11-12):869–873, 2014.
- [60] Diego Pazó, A Carrassi, and Juan M López. Data assimilation by delay-coordinate nudging. *Quarterly Journal of the Royal Meteorological Society*, 142(696):1290–1299, 2016.
- [61] Z. An, D. Rey, J. Ye, and H. D. I. Abarbanel. Estimating the state of a geophysical system with sparse observations: time delay methods to achieve accurate initial states for prediction. *Nonlinear Processes in Geophysics*, 24(1):9–22, 2017.
- [62] Robin C Gilbert, Michael B Richman, Theodore B Trafalis, and Lance M Leslie. Machine learning methods for data assimilation. *Computational Intelligence in Architecturing Complex Engineering Systems*, pages 105–112, 2010.
- [63] Sepp Hochreiter and Jürgen Schmidhuber. Long short-term memory. *Neural computation*, 9(8):1735–1780, 1997.
- [64] Sepp Hochreiter. The vanishing gradient problem during learning recurrent neural nets and problem solutions. *International Journal of Uncertainty, Fuzziness and Knowledge-Based Systems*, 6(02):107–116, 1998.
- [65] Zhong Yi Wan, Pantelis Vlachas, Petros Koumoutsakos, and Themistoklis Sapsis. Data-assisted reduced-order modeling of extreme events in complex dynamical systems. *PloS one*, 13(5), 2018.
- [66] Xiaowei Jia, Jared Willard, Anuj Karpatne, Jordan S Read, Jacob A Zwart, Michael Steinbach, and Vipin Kumar. Physics-guided machine learning for scientific discovery: An application in simulating lake temperature profiles. *arXiv preprint arXiv:2001.11086*, 2020.

- [67] Jaideep Pathak, Zhixin Lu, Brian R Hunt, Michelle Girvan, and Edward Ott. Using machine learning to replicate chaotic attractors and calculate Lyapunov exponents from data. *Chaos: An Interdisciplinary Journal of Nonlinear Science*, 27(12):121102, 2017.
- [68] Artem Chashchin, Mikhail Botchev, Ivan Oseledets, and George Ovchinnikov. Predicting dynamical system evolution with residual neural networks. *arXiv preprint arXiv:1910.05233*, 2019.
- [69] Zhen Chen and Dongbin Xiu. On generalized residue network for deep learning of unknown dynamical systems. *arXiv preprint arXiv:2002.02528*, 2020.
- [70] PR Vlachas, J Pathak, BR Hunt, TP Sapsis, M Girvan, E Ott, and P Koumoutsakos. Backpropagation algorithms and reservoir computing in recurrent neural networks for the forecasting of complex spatiotemporal dynamics. *Neural Networks*, 2020.
- [71] Ziqiao Zhang, Mengxue Hou, Fumin Zhang, and Catherine R Edwards. An LSTM based Kalman Filter for spatio-temporal ocean currents assimilation. In *Proceedings of the International Conference on Underwater Networks & Systems*, pages 1–7, 2019.
- [72] Jianbing Jin, Hai Xiang Lin, Arjo Segers, Yu Xie, and Arnold Heemink. Machine learning for observation bias correction with application to dust storm data assimilation. *Atmospheric Chemistry and Physics*, 19(15):10009–10026, 2019.
- [73] Kelvin Loh, Pejman Shoeibi Omrani, and Ruud van der Linden. Deep learning and data assimilation for real-time production prediction in natural gas wells. *arXiv preprint arXiv:1802.05141*, 2018.
- [74] SHI Xingjian, Zhouong Chen, Hao Wang, Dit-Yan Yeung, Wai-Kin Wong, and Wang-chun Woo. Convolutional LSTM network: A machine learning approach for precipitation nowcasting. In *Advances in Neural Information Processing Systems*, pages 802–810, 2015.
- [75] Francisco J Gonzalez and Maciej Balajewicz. Deep convolutional recurrent autoencoders for learning low-dimensional feature dynamics of fluid systems. *arXiv preprint arXiv:1808.01346*, 2018.
- [76] Arvind Mohan, Don Daniel, Michael Chertkov, and Daniel Livescu. Compressed convolutional LSTM: An efficient deep learning framework to model high fidelity 3D turbulence. *arXiv preprint arXiv:1903.00033*, 2019.
- [77] Romit Maulik, Bethany Lusch, and Prasanna Balaprakash. Reduced-order modeling of advection-dominated systems with recurrent neural networks and convolutional autoencoders. *arXiv preprint arXiv:2002.00470*, 2020.
- [78] Kookjin Lee and Kevin T Carlberg. Model reduction of dynamical systems on nonlinear manifolds using deep convolutional autoencoders. *Journal of Computational Physics*, 404:108973, 2020.
- [79] N Benjamin Erichson, Michael Muehlebach, and Michael W Mahoney. Physics-informed autoencoders for Lyapunov-stable fluid flow prediction. *arXiv preprint arXiv:1905.10866*, 2019.
- [80] Lionel Agostini. Exploration and prediction of fluid dynamical systems using auto-encoder technology.
- [81] Pin Wu, Junwu Sun, Xuting Chang, Wenjie Zhang, Rossella Arcucci, Yike Guo, and Christopher C Pain. Data-driven reduced order model with temporal convolutional neural network. *Computer Methods in Applied Mechanics and Engineering*, 360:112766, 2020.
- [82] Ian Goodfellow, Jean Pouget-Abadie, Mehdi Mirza, Bing Xu, David Warde-Farley, Sherjil Ozair, Aaron Courville, and Yoshua Bengio. Generative adversarial nets. In *Advances in neural information processing systems*, pages 2672–2680, 2014.
- [83] Javad Amirian, Wouter Van Toll, Jean-Bernard Hayet, and Julien Pettr . Data-driven crowd simulation with generative adversarial networks. In *Proceedings of the 32nd International Conference on Computer Animation and Social Agents*, pages 7–10, 2019.
- [84] Edward N Lorenz. Predictability: A problem partly solved. In *Proc. Seminar on Predictability*, volume 1, 1996.
- [85] Henry Abarbanel. *Predicting the future: completing models of observed complex systems*. Springer, 2013.
- [86] William G Whartenby, John C Quinn, and Henry DI Abarbanel. The number of required observations in data assimilation for a shallow-water flow. *Monthly Weather Review*, 141(7):2502–2518, 2013.
- [87] Elana J Fertig, John Harlim, and Brian R Hunt. A comparative study of 4D-VAR and a 4D Ensemble Kalman Filter: perfect model simulations with Lorenz-96. *Tellus A: Dynamic Meteorology and Oceanography*, 59(1):96–100, 2007.
- [88] Peter L Houtekamer and Herschel L Mitchell. A sequential ensemble Kalman filter for atmospheric data assimilation. *Monthly Weather Review*, 129(1):123–137, 2001.

- [89] Edward Ott, Brian R Hunt, Istvan Szunyogh, Aleksey V Zimin, Eric J Kostelich, Matteo Corazza, Eugenia Kalnay, DJ Patil, and James A Yorke. A local ensemble Kalman filter for atmospheric data assimilation. *Tellus A: Dynamic Meteorology and Oceanography*, 56(5):415–428, 2004.
- [90] M Jarak, I M Navon, and M Zupanski. Comparison of sequential data assimilation methods for the Kuramoto–Sivashinsky equation. *International Journal for Numerical Methods in Fluids*, 62(4):374–402, 2010.
- [91] Jeffrey L Anderson and Nancy Collins. Scalable implementations of ensemble filter algorithms for data assimilation. *Journal of Atmospheric and Oceanic Technology*, 24(8):1452–1463, 2007.
- [92] Jacques Blum, François-Xavier Le Dimet, and I Michael Navon. Data assimilation for geophysical fluids. In *Handbook of numerical analysis*, volume 14, pages 385–441. Elsevier, 2009.
- [93] Maziar Raissi and George Em Karniadakis. Hidden physics models: Machine learning of nonlinear partial differential equations. *Journal of Computational Physics*, 357:125–141, 2018.
- [94] Suraj Pawar, Shady E Ahmed, Omer San, and Adil Rasheed. Data-driven recovery of hidden physics in reduced order modeling of fluid flows. *Physics of Fluids*, 32(3):036602, 2020.